NASA CR-132335

ADDITIONAL THREE-DIMENSIONAL BOUNDARY-LAYER COMPUTATIONS FOR A FINITE SWEPT WING

By J. F. Nash
R. M. Scruggs
and W. A. Stevens

Prepared Under Contract No. NAS1-12153 by
LOCKHEED-GEORGIA COMPANY
Marietta, Georgia

for

NATIONAL AERONAUTICS AND SPACE ADMINISTRATION

FOREWORD

This work was performed under Contract NAS1-12153 for the National Aeronautics and Space Administration, Langley Research Center. The Technical Monitor was Dr. R. T. Whitcomb.

CONTENTS

LIST OF TABLES

LIST OF FIGURES

LIST OF FIGURES (Cont'd)

SUMMARY

Additional calculations have been made of the three-dimensional, compressible, turbulent boundary layer on the finite supercritical wing of the NASA modified F8 transonic research airplane. The method was identical to that used in the earlier work, reported in NASA CR-112158, but the calculations were based on the wing pressure distribution measured in flight at $M = 0.90$, instead of on wind tunnel data at $M = 0.50$ and 0.99.

As before, data on the boundary-layer thickness, displacement thickness, skin-friction components, and integrated streamwise skin friction are presented for points along the streamwise stations at which pressure measurements were made.

INTRODUCTION

Reference [1] reports some calculations of the three-dimensional compressible, turbulent boundary layer on the supercritical wing of the NASA modified F8 transonic research airplane. The calculation method was based on the scheme of Nash and Patel [2], [3], but included compressibility effects on the basis of the Crocco integral for temperature. The pressure distributions measured in wind tunnel tests were used but the calculations were done for a higher Reynolds number: 1.5 million per foot. Results were presented for Mach numbers of 0.50 and 0.99.

The flight tests of this airplane have now provided pressure distributions at the actual Reynolds number assumed in the earlier calculations, and NASA requested additional calculations using the new data. The results presented herein are for a Mach number of 0.90.

TECHNICAL APPROACH

The calculations were performed in precisely the same manner as those in the earlier work (Reference [1]). The broad outline of the methodology will be given here for completeness, but the reader is referred to Reference [1] for a detailed treatment.

The turbulent boundary-layer calculation method consisted of the two mean flow momentum equations, expressed in terms of orthogonal curvilinear coordinates, the continuity equation and a pair of rate equations for the turbulent shear stress. The latter are based on the empirically modified turbulent kinetic-energy equation, following the work of Nash and Patel [2], [3]. The Crocco relation for temperature was used to relate local density and mean velocity. The governing equations were integrated, by an explicit numerical scheme, in a three-dimensional domain covering some specified part of the wing surface and extending outwards through, and slightly beyond, the edge of the boundary layer.

As before, the wing was segmented into an inboard and an outboard portion (Figure 1), and a polar coordinate system was fitted to each (Figures 2 through 4). The actual boundary-layer calculations were done in terms of these polar coordinate systems. The pressure data, which were obtained along streamwise measuring stations, had to be interpolated to provide input to the calculations along the arcs and rays of each polar coordinate system. The interpolation was carried out first along the streamwise measuring stations and then along lines of constant percentage

streamwise chord (Figure 5). After the calculations were complete the boundary-layer data were reinterpolated to get back to the original streamwise stations; these reinterpolated results are the data presented herein.

Boundary conditions for the calculations consisted of the conventional ones, at the wing surface and at the outer edge of the boundary layer, together with the side boundary conditions described in Reference [1]. The streamwise stations: 0.044 semispan, on the upper surface, and 0.081 semispan, on the lower surface were treated as planes of symmetry. The inboard, highly-swept, leading edge was taken to be fully turbulent and was also treated as a plane of symmetry. On the outboard portion of the wing, transition from laminar to turbulent flow was assumed to occur at 10% chord; and a simplified laminar calculation was performed to provide initial data for the turbulent boundary layer along the "transition line". The side boundary conditions are illustrated in Figures 6 and 7.

SPECIAL FEATURES OF THE PRESENT CALCULATIONS

Pressure data for the wing, derived from flight measurements on the F8 research airplane, were provided to Lockheed by NASA Langley Research Center. These data consisted of pressure coefficients along six streamwise stations: 0.133, 0.307, 0.458, 0.633, 0.804 and 0.933 semispan, on both the upper and lower surfaces of the wing. In the previous calculations, using wind tunnel data, pressure values were also available at station 0.044 semispan on the upper surface. In order to preserve maximum comparability with the earlier work it was decided to substitute wind tunnel pressure data along the 0.044 semispan station, rather than reduce the size of the computation domain by omitting this station. The required data were obtained from Reference [4] by interpolation between tabulated results at the two closest values of C_L. It emerged later that the pressures along the 0.044 semispan station had little effect on the boundary development further outboard, and thus the procedure adopted was fully justified.

The furthest inboard station on the lower surface coincided with the fuselage junction and pressures along it were derived, as in Reference [1] by extrapolation from the stations 0.133 and 0.307 semispan.

RESULTS

Presentation of the Data

Calculations were performed for a Mach number of 0.90 and a Reynolds number of 1.5 million per foot. The results, presented in Tables 1 and 2 and Figures 8 through 17, consist of the following data:

Displacement thickness, δ^*

Boundary-layer thickness, δ

Spanwise component of skin friction (measured positive inboard), τ_{w_n}

Streamwise component of skin friction, τ_{w_s}

Integrated streamwise skin friction, C_{D_f}

The data are tabulated and plotted versus X_ℓ, the streamwise distance (in inches) from the leading edge, for streamwise stations corresponding to 0.133, 0.307, 0.458, 0.653, 0.804, and 0.933 semispan.

The displacement thickness and boundary-layer thickness are in inches. The skin-friction components are non-dimensionalized by division by twice the free-stream dynamic pressure (i.e., $\rho_\infty Q_\infty^2$). The sectional integrated streamwise skin friction, C_{D_f}, is defined by

$$C_{D_f} = 2\int_0^{X_\ell} \tau_{w_s}\, dX_\ell$$

and has the dimensions of length (inches). It may be related to the conventional sectional skin-friction coefficient, C_{d_f}, by

$$C_{d_f} = \frac{C_{D_f}}{c}$$

where c is the local streamwise chord.

Contour plots of boundary-layer thickness are presented in Figure 16, for each surface of the wing. Figure 17 shows a map of the skin-friction vectors at selected points on the wing. The vectors are drawn to scale, with an arrow one inch long representing a skin-friction vector of magnitude $0.005\ \rho_\infty Q_\infty^2$.

Discussion

As in the earlier work (Reference [1]), the boundary layer was predicted to remain attached over the whole of the upper surface. This time, however, flow separation was predicted to occur, on the lower surface, over part of the outboard wing. Separation is defined, here, as the condition where the component of skin friction, normal to the lines on constant percentage of local chord, falls to zero. This condition was reached, almost simultaneously at several spanwise positions, at about 0.85 of the local streamwise chord, and the outboard-wing calculation did not proceed beyond that point.

Figure 12 shows the spanwise variation of boundary-layer thickness, and Figure 13 shows the corresponding variation of displacement thickness. Data from Reference [1] are shown for comparison. The data in Figures 12

and 13 all relate to conditions at the trailing edge, except for the present lower surface results which are for a position just ahead of the separation line. The results of Reference [1] indicate that, on the lower surface, the boundary-layer thicknesses decrease as the trailing edge is approached due to a strong favorable pressure gradient, and most of the difference between those data and the present results for the lower surface is due to the difference in chordwise position.

The difference between the boundary-layer thickness, on the upper surface, is more significant. Figures 12 and 13 show that the boundary layer is thicker, over the inboard portion of the wing and has a larger displacement thickness than was found in the earlier calculations. The increased thickness predicted in the present calculations are associated with a redistribution of the boundary-layer air on the inboard wing and are indicative of the sensitivity of this type of flow to details of the pressure distribution. Nearer the wing tip the present data correlate well with the earlier results at $M = 0.99$.

The spanwise distribution of the integrated skin friction is entirely consistent with the results of Reference [1], (Figure 14). It is assumed that there is no contribution to the skin-friction integral between the separation line, on the lower surface, and the trailing edge. Because of this, and also because of the low values of skin friction ahead of separation, the present values of C_D are slightly smaller, on the outboard lower surface, than the earlier results. The sectional skin-friction coefficients (Figure 15) show the same trend, but are otherwise unremarkable.

The skin-friction drag coefficient for the wing is about 0.0065, based on the partial plan areas of 24,900 sq. in. for the upper surface and 20,200 sq. in. for the lower surfaces. The comparable figures from Reference [1] are 0.0063, at M = 0.50, and 0.0071 at M = 0.99.

There is no conflict between the observations of a thicker boundary layer, in the present calculations, but little difference in the computed values of skin-friction drag. The form drag of the wing would almost certainly be higher than that for the earlier results--both because of the thicker boundary layer on the upper surface and because of the separation on the lower surface.

The contour plots of boundary-layer thickness (Figure 16) indicate a very regular development of the boundary layer over the wing. The local peaks in boundary-layer thickness, detected on the inboard wing in the calculations of Reference [1], are no longer present. The map of skin-friction vectors (Figure 17) shows significant differences from the earlier results with regard to the direction of the local surface flow. The present data exhibit outflow, in the boundary layer, over the whole of upper surface inboard of roughly 50% semispan. This is in contrast to areas of strong inflow (i.e., flow towards the fuselage) detected in the results of Reference [1]. The fact that the peaks in boundary-layer thickness, and the regions of inflow, are now both absent lends support to the earlier conclusion that the two phenomena were closely linked. On the lower surface there is outflow over the whole wing. The aft row of skin-friction vectors, on the outboard lower surface, are just ahead of the separation line, and it will be noted that in this region the vectors lie almost parallel to the trailing edge.

CONCLUSIONS

Additional calculations have been made of the three-dimensional compressible turbulent boundary layer on the finite supercritical wing of the NASA modified F8 transonic research airplane. The present results are for a Mach number of 0.9, and are based on the surface pressure distributions measured in flight. They complement the results of Reference [1], which were based on wind tunnel pressures and corresponded to Mach numbers of 0.5 and 0.99.

Analysis of the results indicates both similarities and differences between the present data and the data presented in Reference [1]. The boundary-layer calculation method was precisely the same as that used in the earlier work. A compressible version of the method of Nash and Patel [2], [3], and the computations were organized in precisely the same way. Therefore, the difference in predicted boundary-layer behavior have to be interpreted as being due to subtle differences in the surface pressure distributions (and, of course, to a small extent, due to the difference in Mach number).

The skin-friction drag data for the whole wing, and the spanwise variation of skin-friction drag, correlate well with the earlier results. The boundary-layer thicknesses, however, are generally greater than those calculated in the earlier work. The difference is most marked on the inboard wing, where the streamwise variation of boundary-layer thickness is now more regular and shows no evidence of the local peaks observed in the data of Reference [1]. The special variations of surface-flow direction are also

more regular on the inboard wing. The present calculations indicate separation on the outboard lower surface at about 0.85 of local streamwise chord, whereas, in the earlier work, the flow was shown to remain attached over the whole wing.

REFERENCES

1. J. F. Nash and R. M. Scruggs: "Three-Dimensional Compressible Boundary-Layer Computations for a Finite Swept Wing", NASA CR-112158, 1972.

2. J. F. Nash and V. C. Patel: "A Generalized Method for the Calculation of Three-Dimensional Turbulent Boundary Layers", Project SQUID Symposium, Georgia Institute of Technology, 1971.

3. J. F. Nash and V. C. Patel: "Three-Dimensional Turbulent Boundary Layers", SBC Technical Books, 1972.

4. C. D. Harris: "Wind-Tunnel Measurements of Aerodynamic Load Distribution on a NASA Supercritical-Wing Research Airplane Configuration", NASA TMX-2469, 1972. (Title unclassified, paper classified).

TABLE 1 - UPPER SURFACE

X_ℓ	δ^*	δ	τ_{w_n}	τ_{w_s}	$\frac{1}{2}C_{D_f}$
		0.133 Semispan			
0.12	.0095	.0935	.000635	.001776	.00000
5.85	.0108	.1015	-.000256	.002201	.01145
10.16	.0120	.1089	-.000906	.002465	.02150
14.49	.0132	.1173	-.001540	.002694	.03270
19.99	.0150	.1708	-.001473	.002659	.04745
25.32	.0200	.2079	-.001479	.002622	.06150
29.60	.0232	.2244	-.001501	.002608	.07271
35.33	.0311	.2549	-.001466	.002470	.08722
39.72	.0352	.2988	-.001358	.002363	.09787
45.71	.0435	.3752	-.001194	.002218	.11157
50.30	.0529	.4262	-.001086	.002122	.12151
54.98	.0639	.4735	-.000992	.002038	.13124
59.71	.0743	.5174	-.000933	.002019	.14085
64.55	.0849	.5606	-.000922	.002011	.15059
69.44	.0934	.5987	-.000953	.002017	.16045
74.44	.0973	.6404	-.001030	.002020	.17396
80.75	.0995	.6646	-.001045	.001995	.18326
84.23	.1082	.6968	-.001014	.001862	.18996
89.42	.1259	.7555	-.000891	.001727	.19927
94.56	.1489	.8288	-.000772	.001634	.20789
99.88	.1721	.9060	-.000681	.001561	.21638
109.18	.1943	1.0072	-.000612	.001498	.23049
120.86	.1987	1.0729	-.000611	.001484	.24794
130.85	.2101	1.1426	-.000592	.001449	.26260
138.95	.2231	1.2145	-.000571	.001462	.27436
147.72	.2405	1.3041	-.000572	.001473	.28723
162.46	.3132	1.5286	-.000554	.001377	.30852
173.91	.3846	1.7215	-.000505	.001225	.32337
182.86	.4347	1.8609	-.000463	.001140	.33395
		0.307 Semispan			
10.45	.0151	.1099	.000922	.003727	.00480
15.09	.0256	.1563	.000912	.003353	.02111
20.15	.0448	.2393	.000457	.002858	.03677
24.66	.0607	.3109	.000174	.002559	.04897
29.66	.0769	.3910	.000009	.002427	.06136
35.04	.0897	.4661	-.000083	.002406	.07436
39.93	.1031	.5295	-.000203	.002295	.08585
44.01	.1247	.6115	-.000257	.002086	.09476

TABLE 1 - UPPER SURFACE (Cont'd)

X_ℓ	δ^*	δ	τ_{w_n}	τ_{w_s}	$\frac{1}{2}C_{D_f}$
		0.307 Semispan (Cont'd)			
50.99	.1581	.7511	-.000287	.001813	.10811
56.54	.1636	.8307	-.000213	.001838	.11823
59.50	.1712	.8827	-.000196	.001826	.12367
66.22	.1986	1.0205	-.000171	.001784	.13576
73.56	.2464	1.1984	-.000200	.001677	.14352
81.32	.3314	1.4357	-.000301	.001415	.16063
92.00	.5989	1.9410	-.000452	.000879	.17281
		0.458 Semispan			
9.23	.0100	.0397	.001199	.006040	.00605
11.00	.0167	.0674	.000946	.005422	.01614
15.18	.0322	.1364	.000528	.004505	.03692
20.29	.0597	.2256	-.000163	.003134	.05689
25.19	.1018	.3457	-.000493	.002118	.06917
29.57	.1289	.4607	-.000462	.001845	.07764
35.25	.1369	.5772	-.000307	.001858	.08804
40.84	.1432	.6710	-.000214	.001866	.09857
45.01	.1583	.7506	-.000200	.001796	.10619
49.91	.1653	.8243	-.000138	.001821	.11497
55.41	.1645	.8894	-.000036	.001952	.12531
61.62	.1690	.9670	.000033	.002080	.13790
71.78	.2479	1.1923	-.000210	.001609	.15734
81.21	.4227	1.5611	-.000378	.001101	.16930
		0.653 Semispan			
7.55	.0087	.0352	.001338	.005548	.00523
10.24	.0187	.0778	.000813	.004197	.01810
14.97	.0386	.1588	.000275	.002790	.03439
19.85	.0619	.2548	.000051	.002146	.04608
25.31	.0781	.3578	.000100	.002059	.05734
30.32	.0860	.4352	.000138	.002130	.06788
35.05	.0978	.5070	.000187	.002099	.07792
40.84	.1133	.5939	.000188	.002078	.08985
45.34	.1099	.6373	.000361	.002391	.09979
50.42	.1188	.6977	.000348	.002397	.11207
55.80	.1413	.7741	.000193	.002110	.12428
61.84	.2041	.9046	-.000114	.001478	.13536
66.44	.2955	1.0796	-.000248	.001078	.14105

TABLE 1 - UPPER SURFACE (Cont'd)

X_ℓ	δ^*	δ	τ_{w_n}	τ_{w_s}	$\frac{1}{2}C_{D_f}$
		0.804 Semispan			
6.32	.0081	.0352	.000780	.004323	.00381
10.10	.0222	.1004	.000374	.002974	.01687
14.92	.0366	.1768	.000307	.002614	.03048
20.27	.0538	.2598	.000214	.002339	.04360
25.39	.0664	.3357	.000220	.002264	.05532
30.85	.0769	.4103	.000254	.002253	.06761
35.21	.0818	.4628	.000338	.002371	.07764
40.06	.0899	.5202	.000355	.002360	.08931
45.69	.1114	.5981	.000219	.002013	.10160
49.19	.1291	.6529	.000121	.001787	.10827
55.65	.2092	.8205	-.000151	.001136	.11774
		0.933 Semispan			
5.23	.0070	.0300	.000831	.004503	.00367
10.07	.0232	.1105	.000471	.003293	.02143
15.39	.0474	.2032	.000019	.002251	.03607
19.97	.0651	.2868	-.000020	.001909	.04525
25.50	.0644	.3549	.000229	.02170	.05659
29.75	.0644	.3980	.000381	.02355	.06631
34.90	.0804	.4651	.000272	.002053	.07789
40.66	.1053	.5489	.000125	.001695	.08869
46.00	.1435	.6433	-.000074	.001203	.09673

TABLE 2 - LOWER SURFACE

X	δ^*	δ	τ_{w_n}	τ_{w_s}	$\frac{1}{2}C_{D_f}$
		0.133 Semispan			
0.00	.0141	.0726	.000549	.001975	.00000
5.33	.0217	.1174	.000347	.001924	.01050
9.54	.0315	.1755	.000250	.001818	.01838
15.02	.0511	.2708	.000189	.001689	.02800
21.38	.0669	.3641	.000123	.001622	.03847
24.73	.0726	.4025	.000090	.001606	.04388
31.60	.0838	.4750	.000029	.001611	.05490
35.12	.0899	.5120	.000000	.001622	.06058
38.68	.0954	.5497	-.000033	.001634	.06639
45.95	.1000	.6124	-.000111	.001668	.07838
49.65	.1019	.6522	-.000166	.001696	.08459
55.81	.1037	.6769	-.000210	.001688	.09501
59.47	.1055	.7003	-.000235	.001676	.10117
70.60	.1116	.7708	-.000265	.001636	.11960
78.17	.1175	.8254	-.000253	.001606	.13186
89.70	.1276	.9376	-.000243	.001629	.15057
101.36	.1434	1.0718	-.000228	.001613	.16950
109.87	.1686	1.1860	-.000197	.001473	.18267
121.65	.2225	1.4045	-.000119	.001295	.19894
129.44	.2647	1.5696	-.000071	.001187	.20861
141.41	.3415	1.8543	-.000029	.000989	.22159
149.62	.3929	2.0570	-.000014	.000874	.22923
162.62	.3585	2.2026	-.000008	.001056	.24127
171.95	.3214	2.2614	-.000049	.001237	.25198
		0.307 Semispan			
10.45	.0162	.1459	-.000178	.002108	.00500
15.13	.0228	.1930	.000047	.002020	.01455
19.80	.0317	.2681	.000049	.001955	.02381
25.43	.0442	.3560	-.000004	.001816	.03443
29.79	.0524	.4260	-.000012	.001779	.04224
35.35	.0588	.5220	.000006	.001760	.05206
40.37	.0606	.6267	.000034	.001793	.06099
46.85	.0823	.7977	-.000051	.001610	.07223
54.36	.1050	.9744	-.000079	.001505	.08374
62.99	.2054	1.3030	-.000244	.001061	.09467
75.75	.4851	1.9554	-.000337	.000616	.10541

TABLE 2 - LOWER SURFACE (Cont'd)

X	δ^*	δ	τ_{w_n}	τ_{w_s}	$\frac{1}{2}C_{D_f}$
		0.458 Semispan			
9.23	.0070	.0331	-.000460	.002496	.00432
12.00	.0172	.0945	-.000341	.002173	.01076
14.89	.0258	.1479	-.000291	.002025	.01683
20.09	.0397	.2348	-.000229	.001878	.02693
25.25	.0522	.3166	-.000199	.001788	.03638
29.85	.0618	.3852	-.000173	.001742	.04449
35.25	.0723	.4649	-.000158	.001680	.05440
39.30	.0823	.5299	-.000162	.001618	.06045
45.67	.1065	.6525	-.000201	.001451	.07014
50.42	.1276	.7512	-.000228	.001332	.07678
55.60	.1582	.8758	-.000264	.001212	.08336
61.17	.2360	1.0786	-.000351	.000967	.08950
66.40	.5595	1.5522	-.0000468	.000428	.09335
		0.653 Semispan			
7.55	.0068	.0320	-.000289	.002601	.00370
10.09	.0156	.0826	-.000201	.002305	.00992
15.31	.0329	.1768	-.000195	.001955	.02097
19.85	.0465	.2559	-.000188	.001813	.02947
25.53	.0590	.3436	-.000146	.001773	.03960
30.63	.0731	.4245	-.000159	.001681	.04843
35.53	.0947	.5171	-.000222	.001507	.05629
39.26	.1235	.6102	-.000294	.001303	.06151
45.49	.1843	.7937	-.000360	.001038	.06873
50.05	.2481	.9597	-.00396	.000865	.07308
54.59	.4039	1.2543	-.000414	.000652	.07653
		0.804 Semispan			
6.32	.0063	.0294	-.000256	.002602	.00332
10.21	.0193	.1036	-.000153	.002174	.01250
15.38	.0355	.1932	-.000148	.001910	.02300
20.46	.0498	.2772	-.000139	.001794	.03235
25.66	.0641	.3605	-.000141	.001698	.04144
29.76	.0771	.4293	-.000165	.001611	.04823
35.21	.1196	.5655	-.000298	.001278	.05615
40.06	.1969	.7527	-.000406	.000949	.06153
45.73	.3526	1.0782	-.000469	.000669	.06606

TABLE 2 - LOWER SURFACE (Cont'd)

X	δ^*	δ	τ_{w_n}	τ_{w_s}	$\frac{1}{2}C_{D_f}$
		0.933 Semispan			
5.23	.0057	.0263	-.000157	.002820	.00314
9.90	.0215	.1132	-.000099	.002236	.01476
14.90	.03818	.2013	-.000141	.001934	.02507
19.97	.0512	.2827	-.000124	.001850	.03465
24.60	.0667	.3618	-.000168	.001703	.04288
30.00	.1083	.4929	-.000328	.001284	.05107
34.65	.2059	.7039	-.000452	.000871	.05599
37.87	.3055	.8997	-.000488	.000700	.05851

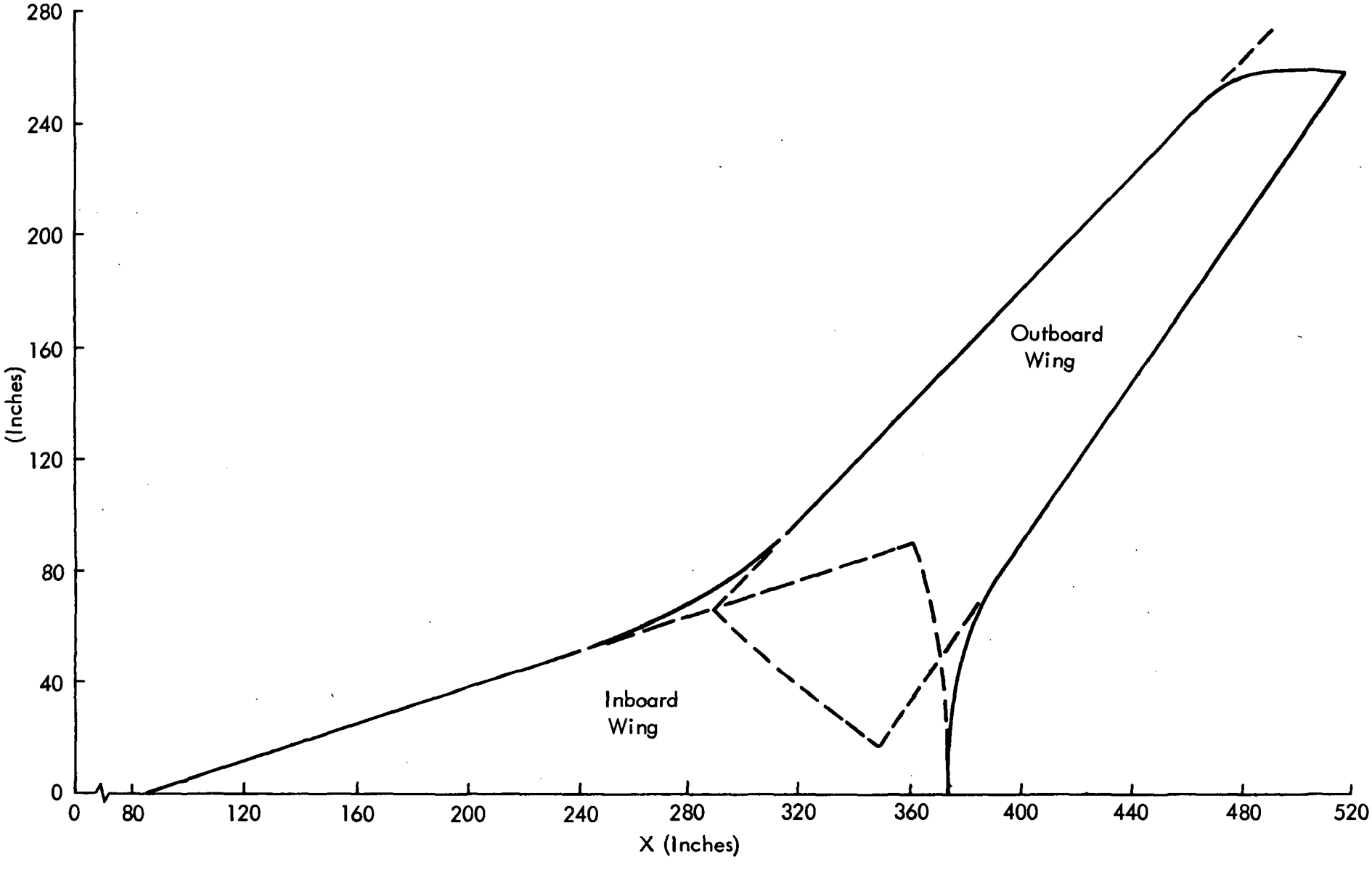

Figure 1. Segmentation of the Wing

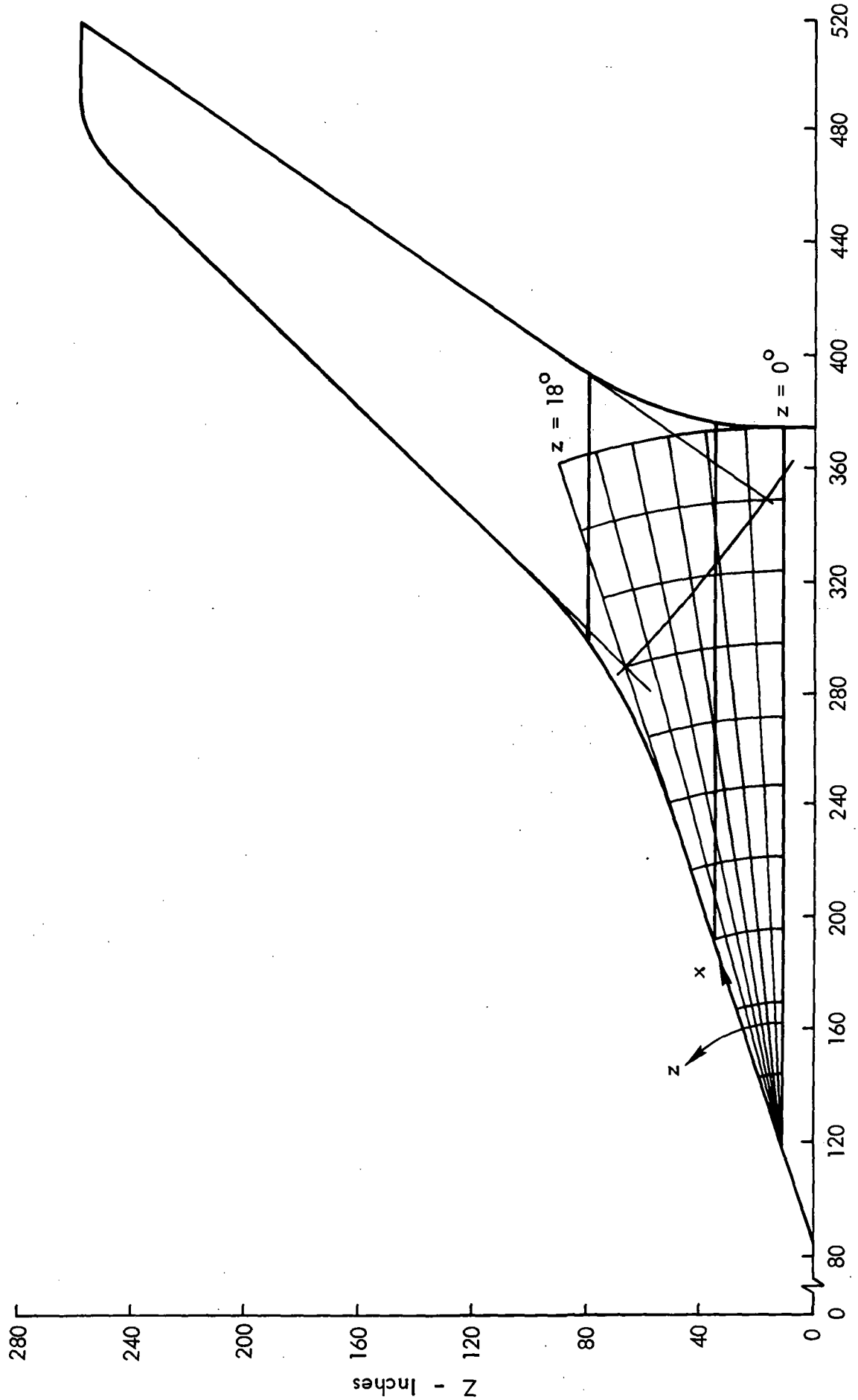

Figure 2. Upper Surface Inboard Coordinate System

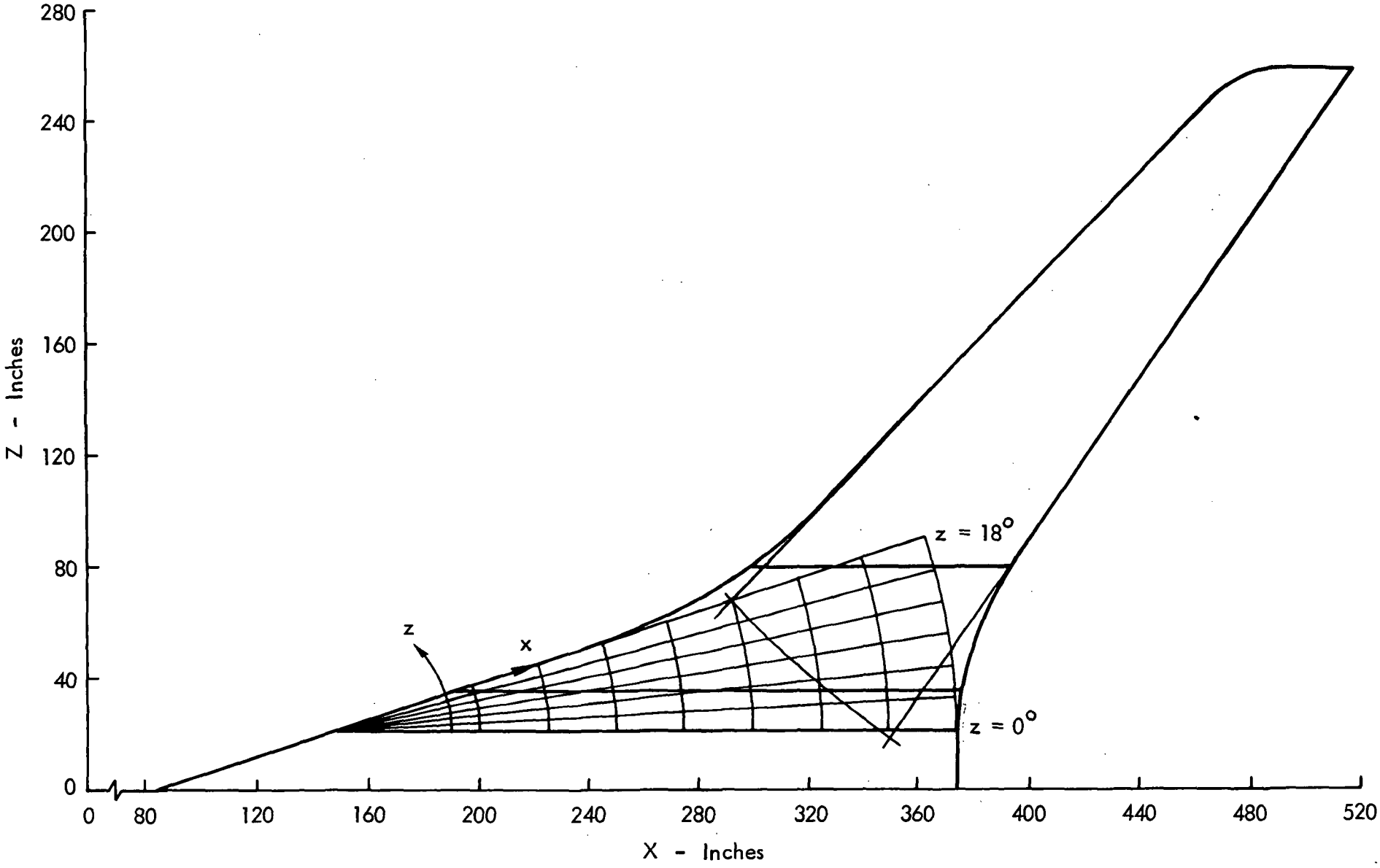

Figure 3. Lower Surface Inboard Coordinate System

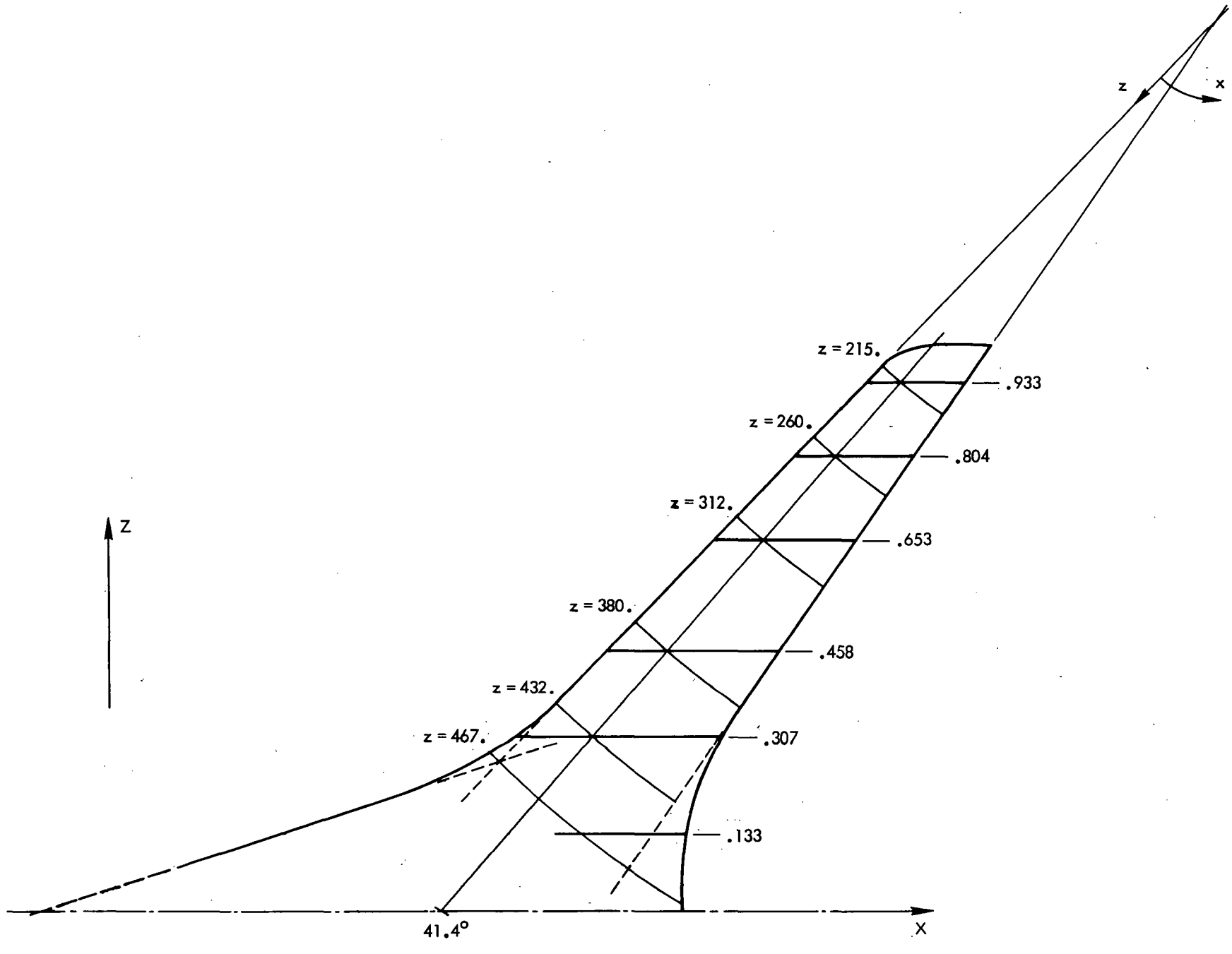

Figure 4. Outboard Coordinate System

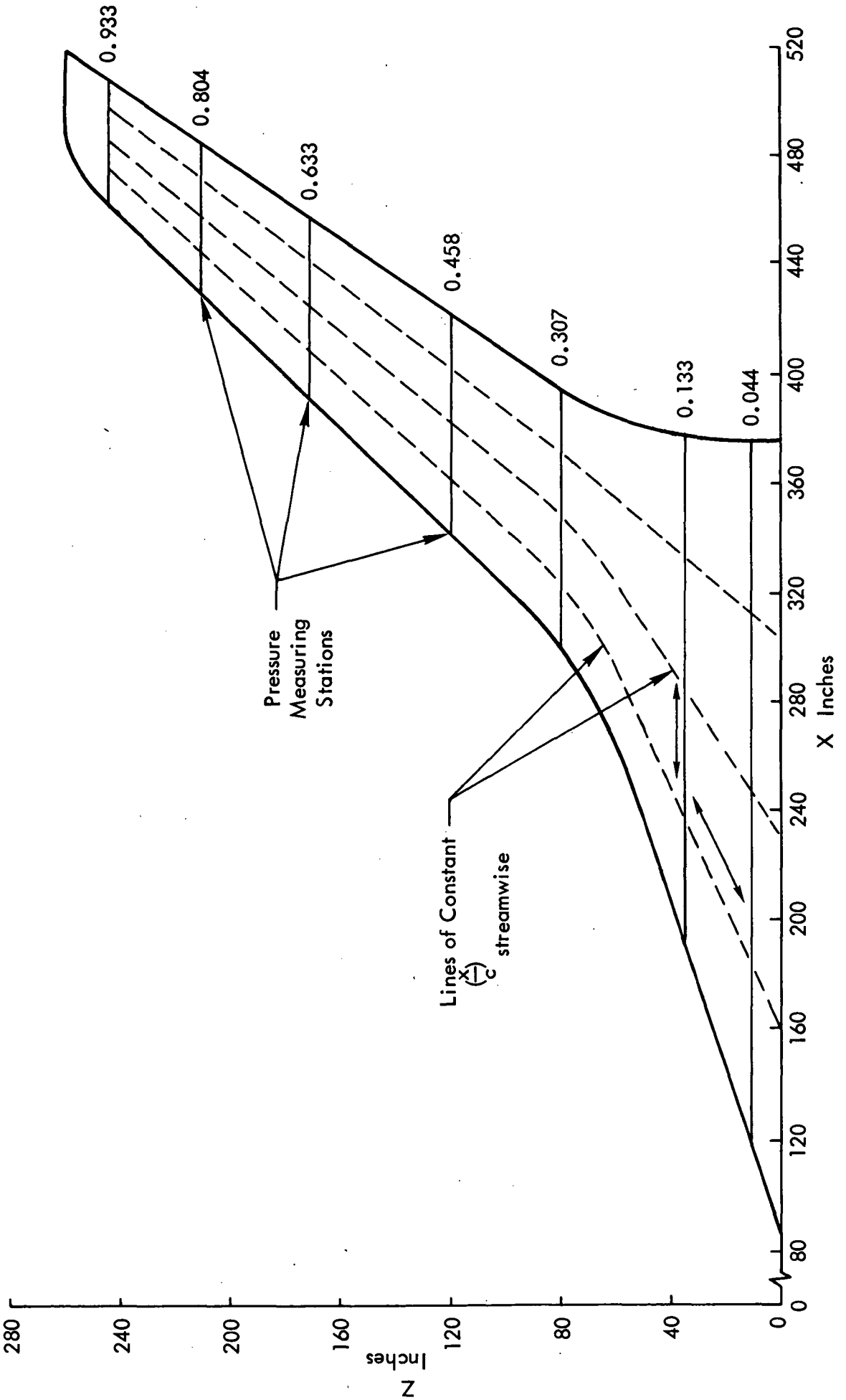

Figure 5. Method of Interpolating the Pressure Data

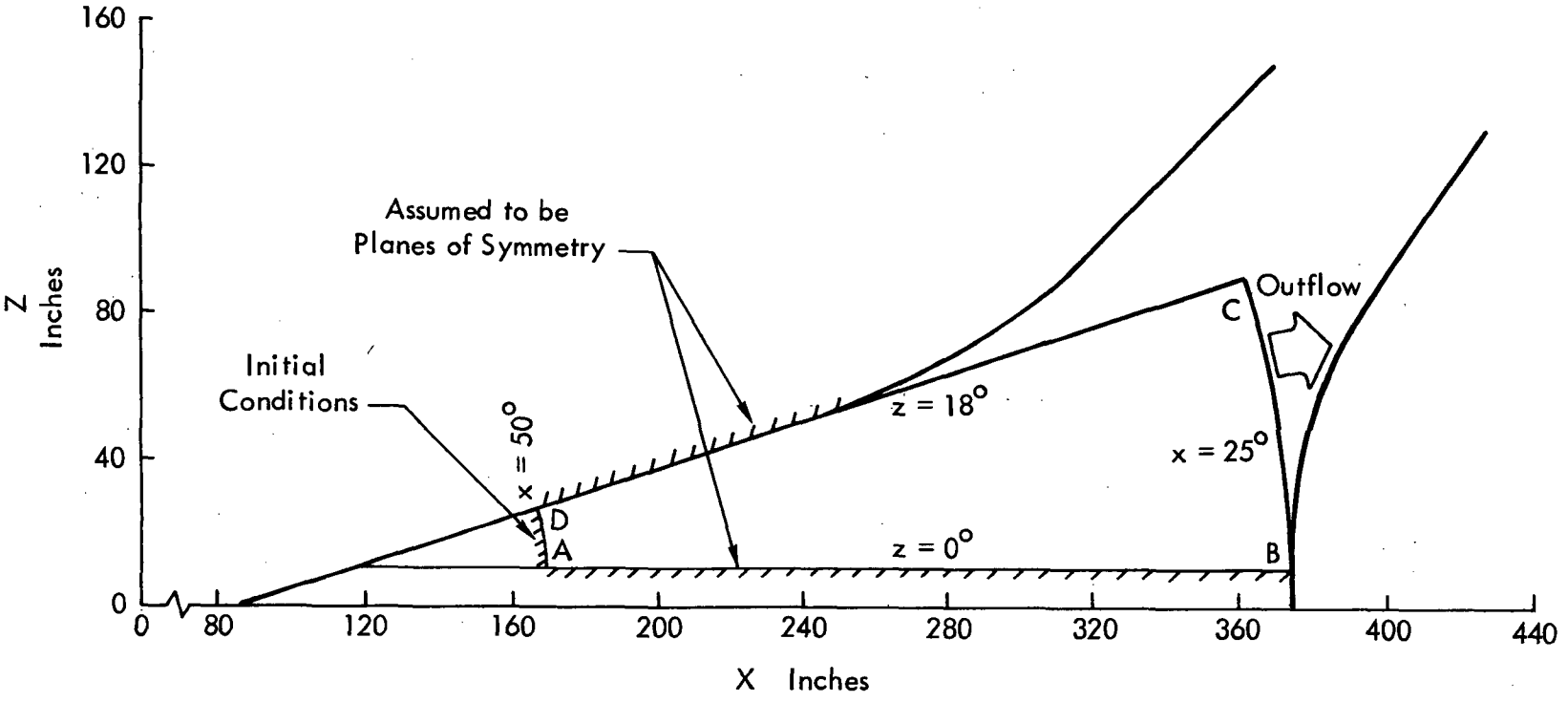

Figure 6. Boundary Conditions for the Inboard Calculation

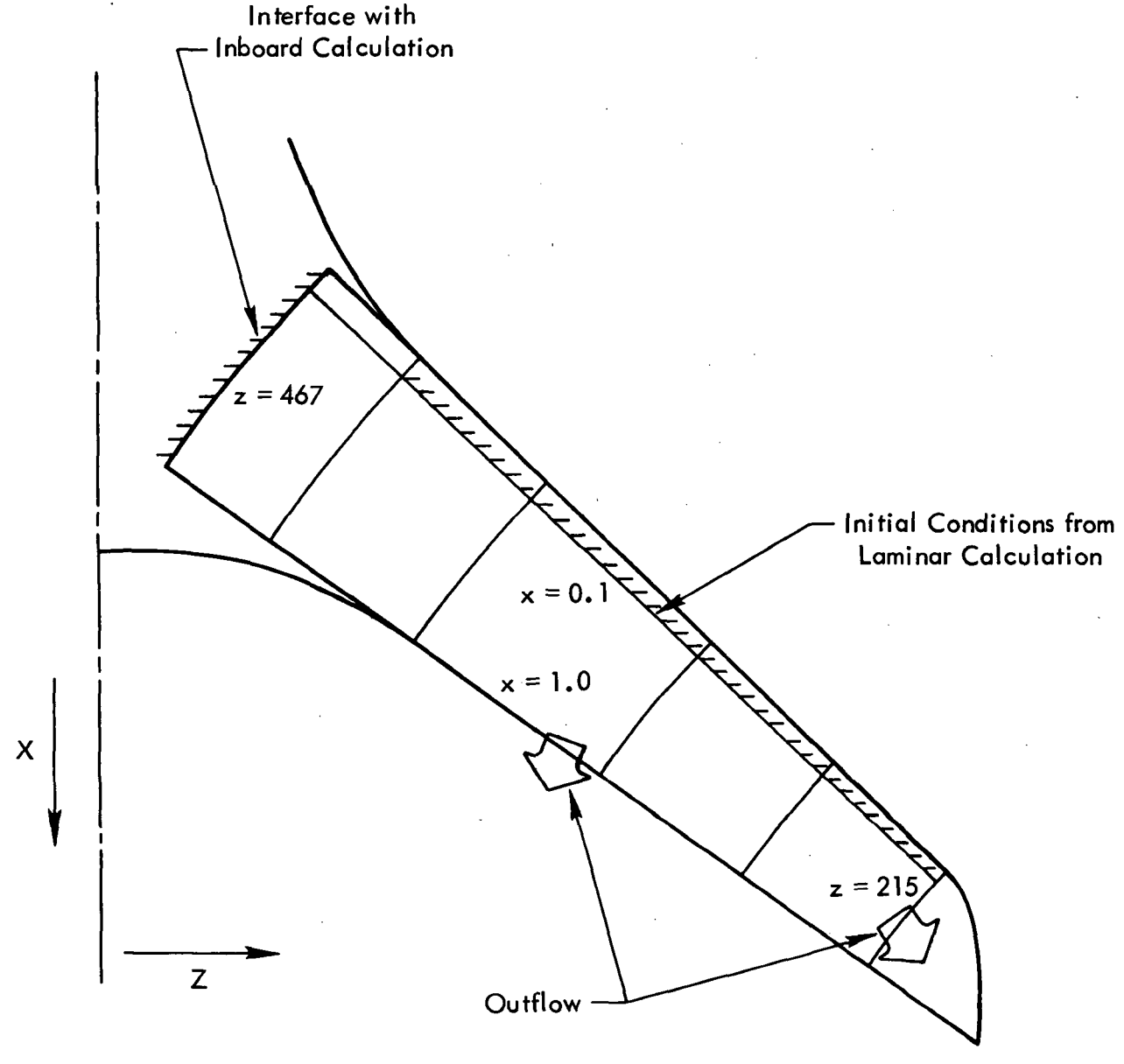

Figure 7. Boundary Conditions for the Outboard Calculation

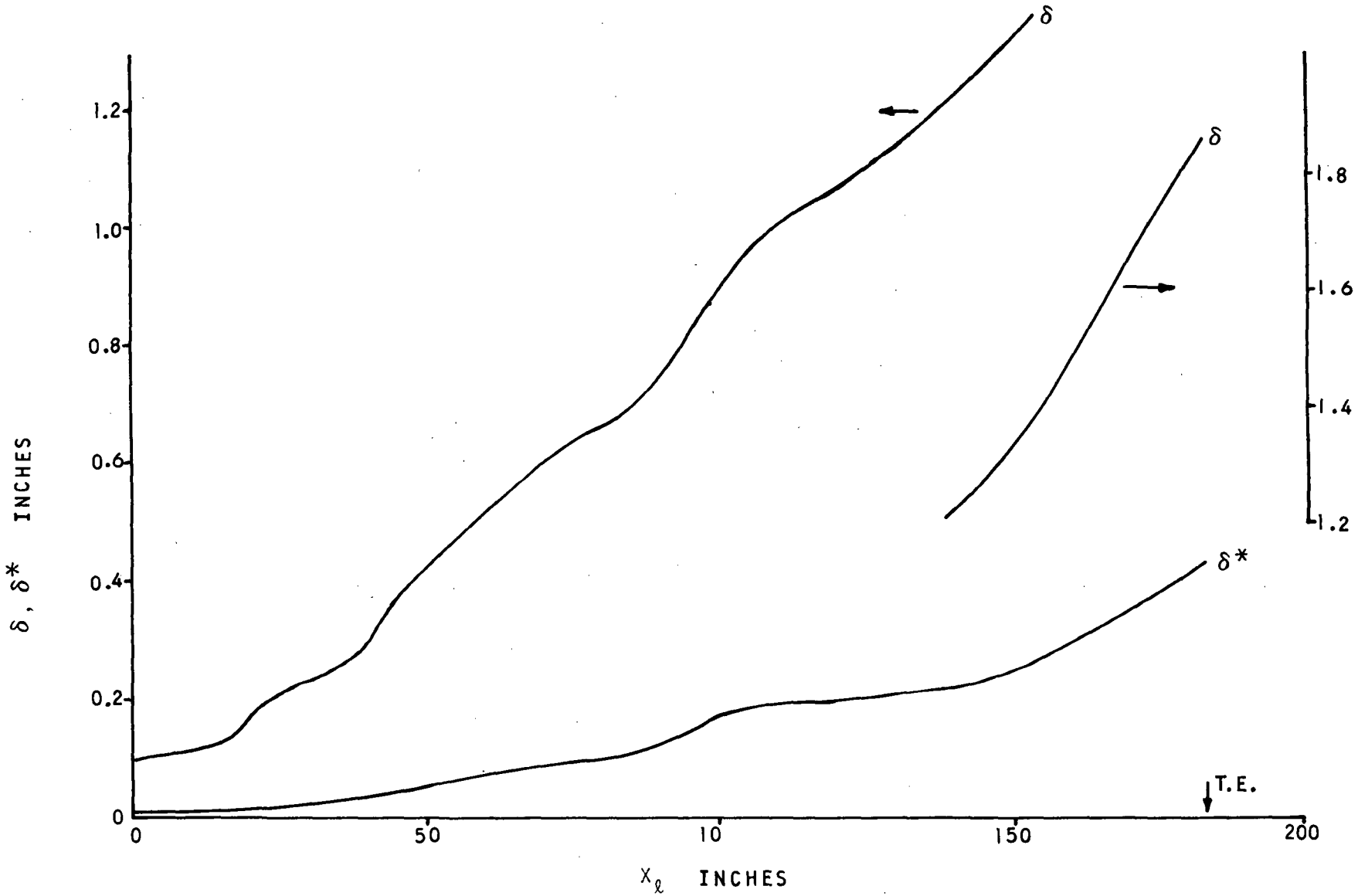

FIGURE 3 BOUNDARY-LAYER THICKNESS AND DISPLACEMENT THICKNESS, UPPER SURFACE: 0.133 SEMISPAN

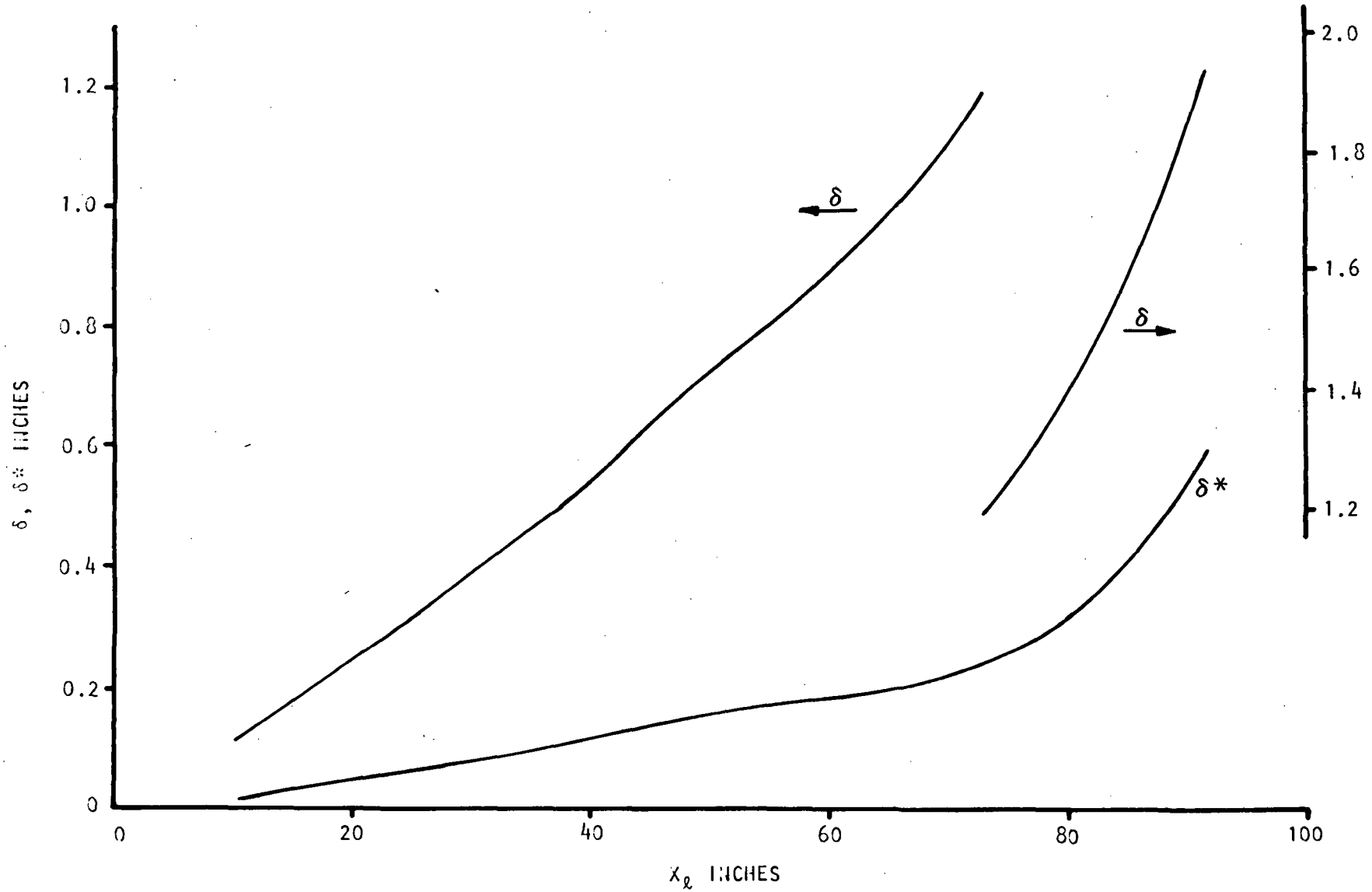

FIGURE 8 (Cont'd): 0.307 SEMISPAN

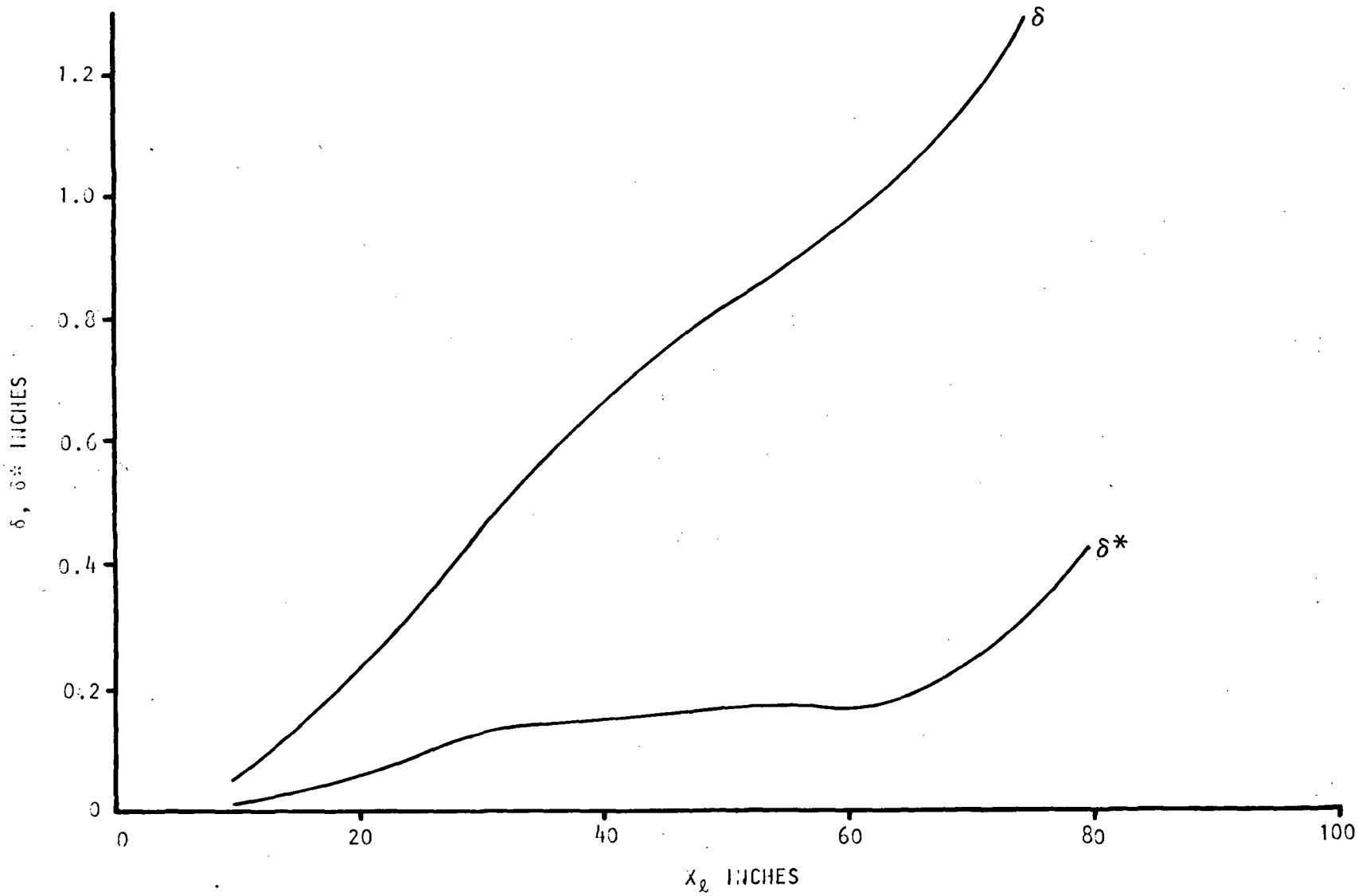

FIGURE 8 (Cont'd): 0.458 SEMISPAN

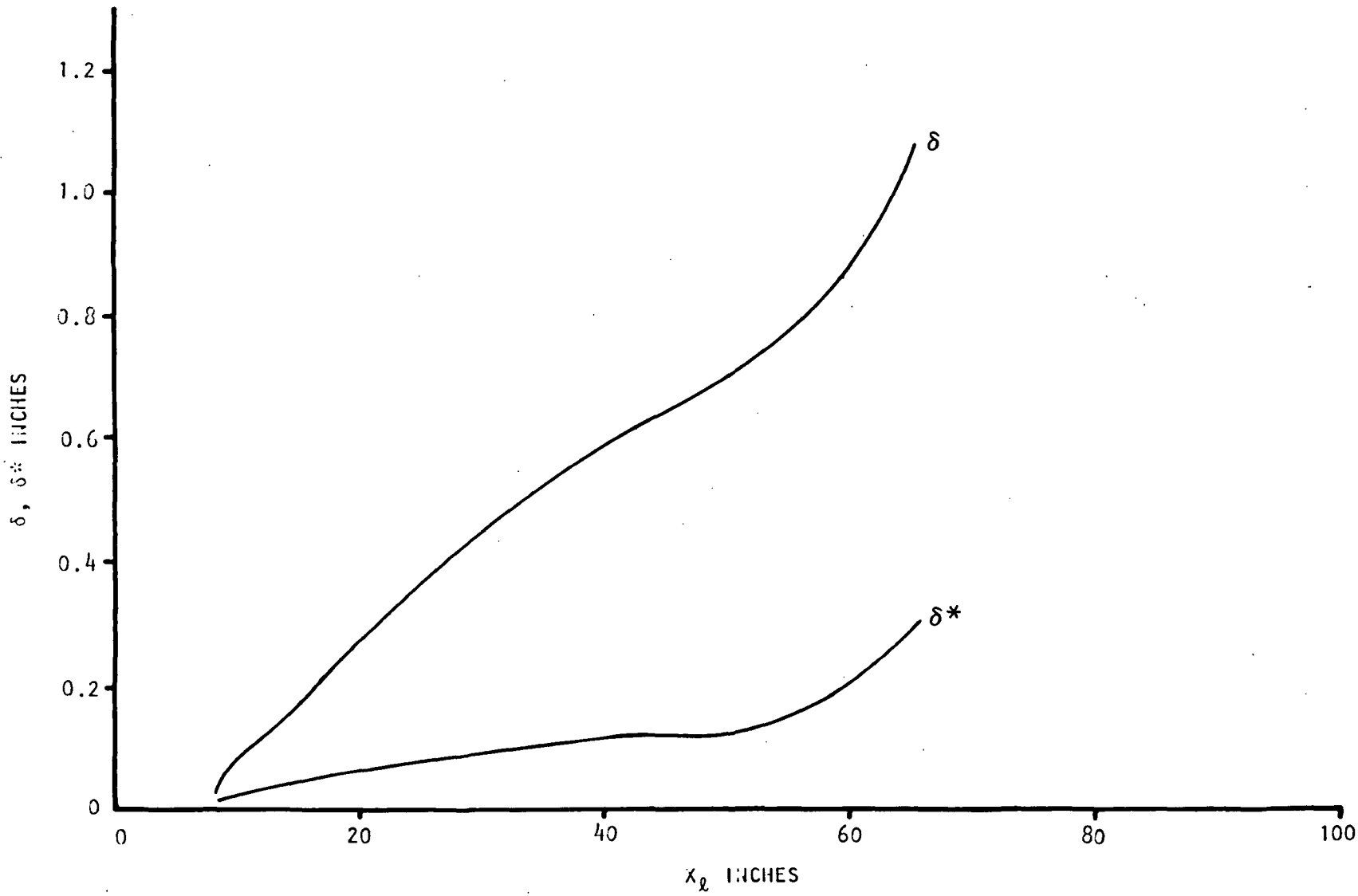

FIGURE 8 (Cont'd): 0.653 SEMISPAN

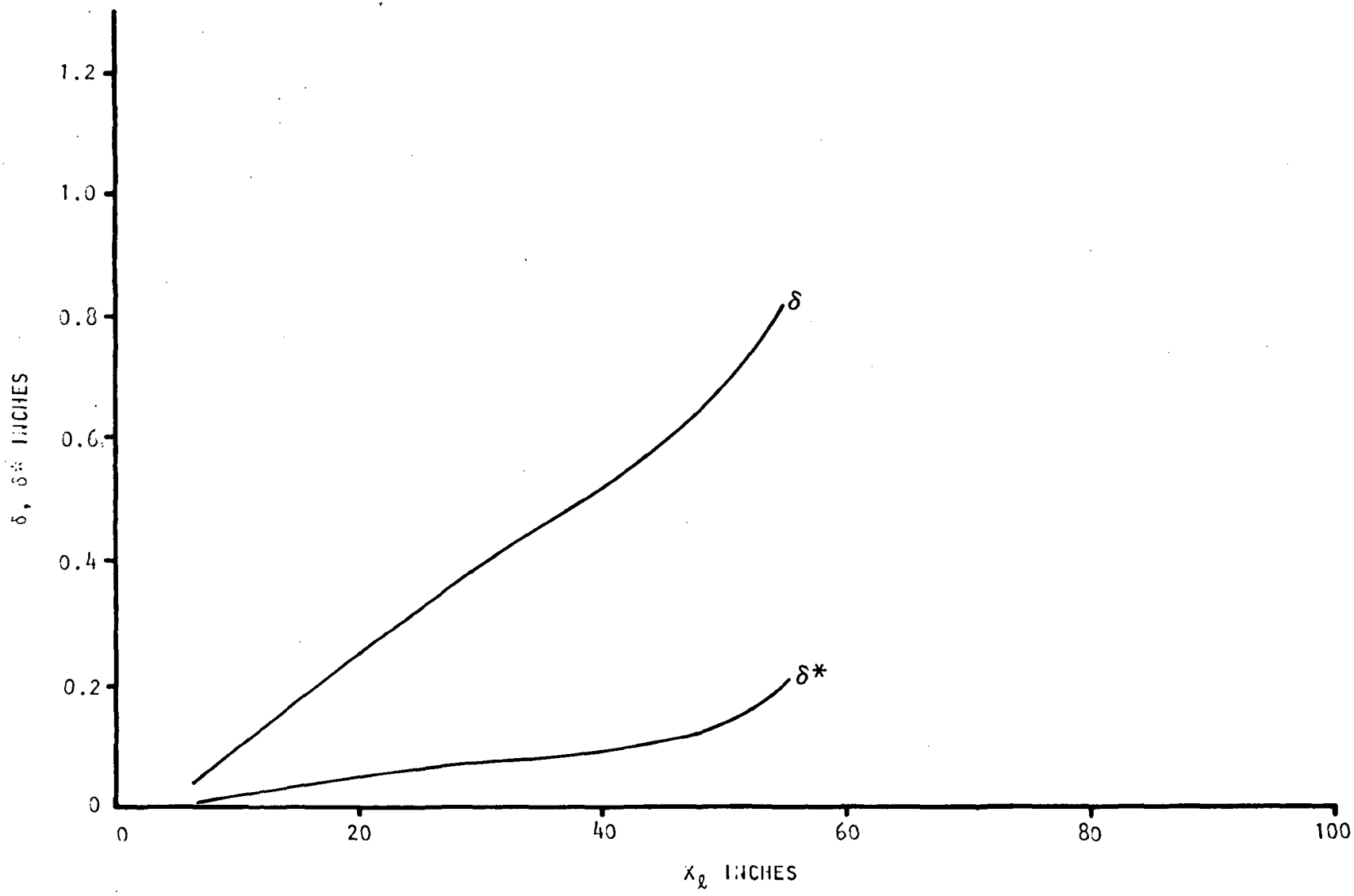

FIGURE 8 (Cont'd): 0.804 SEMISPAN

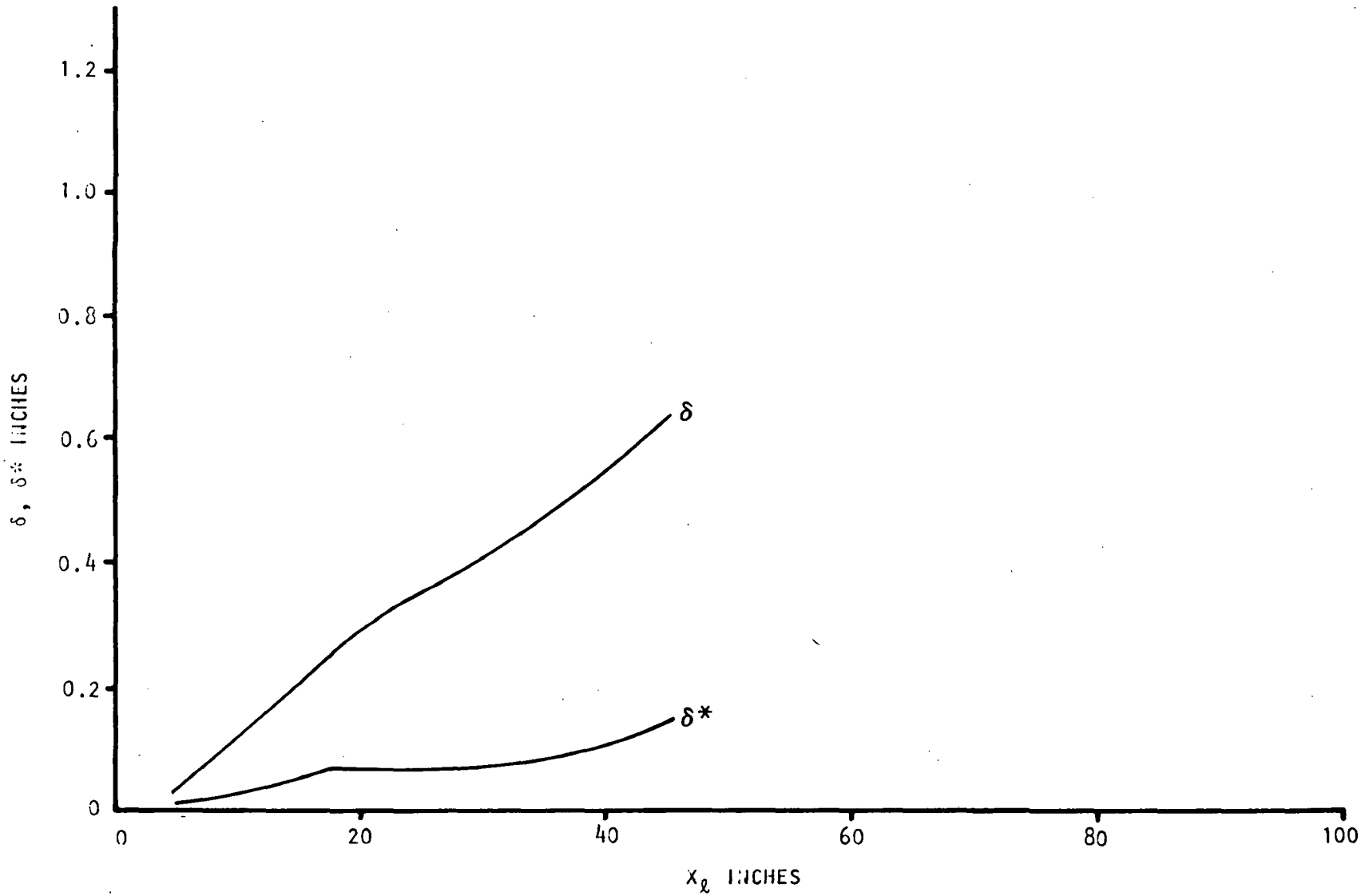

FIGURE 8 (Cont'd): 0.933 SEMISPAN

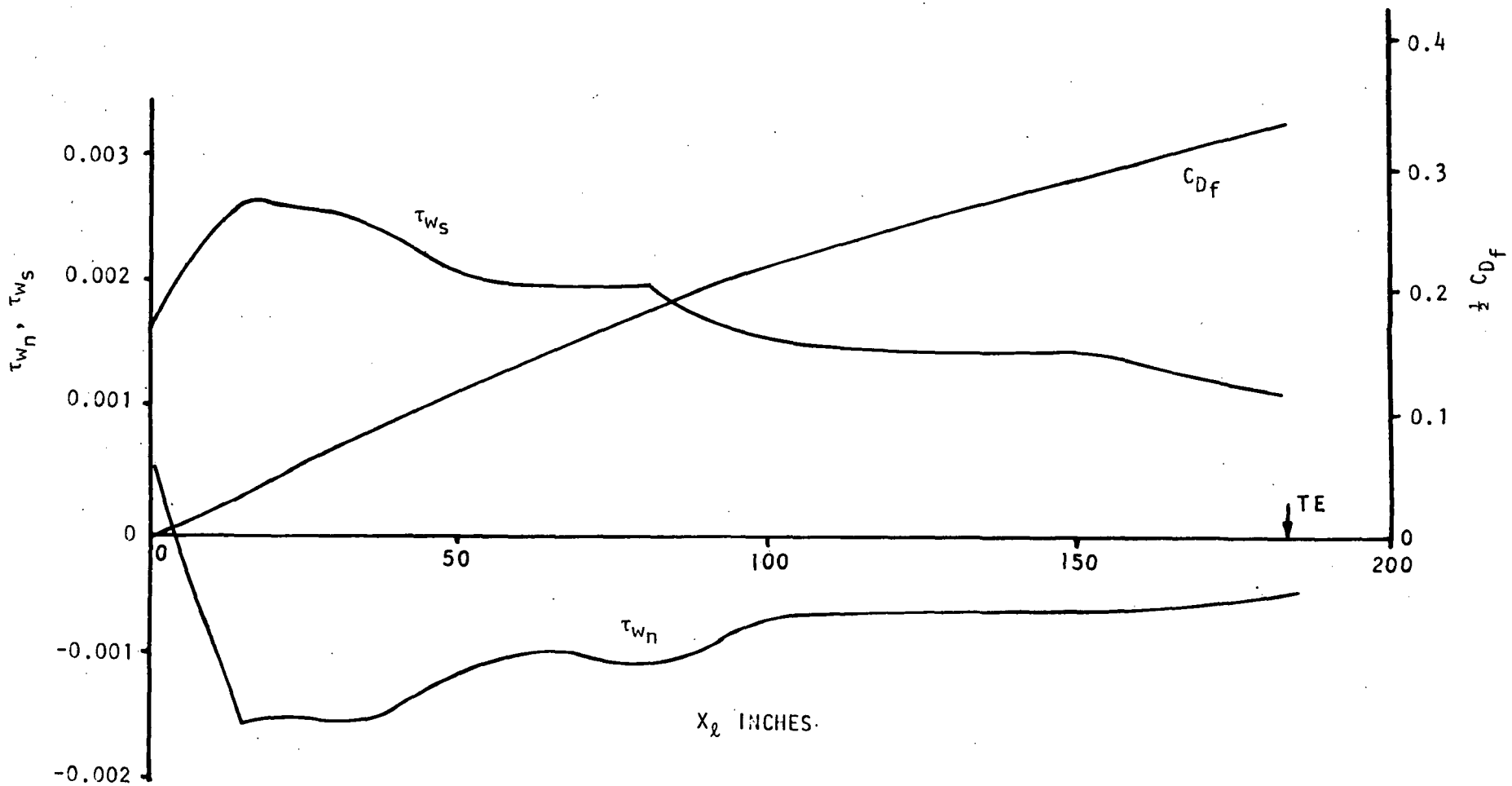

FIGURE 9 SKIN-FRICTION COMPONENTS AND INTEGRATED STREAMWISE SKIN FRICTION, UPPER SURFACE: 0.133 SEMISPAN

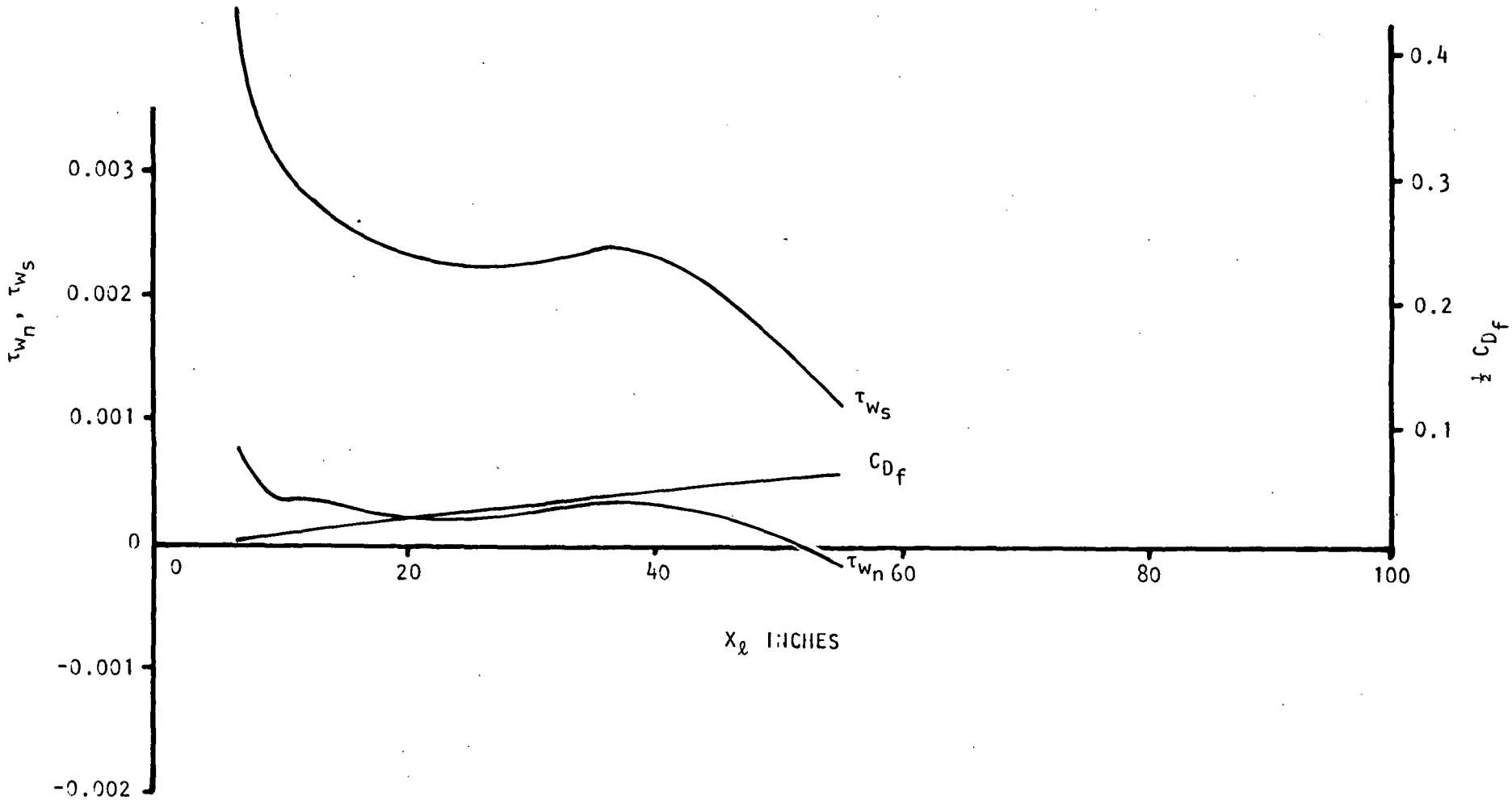

FIGURE 9 (Cont'd): 0.804 SEMISPAN

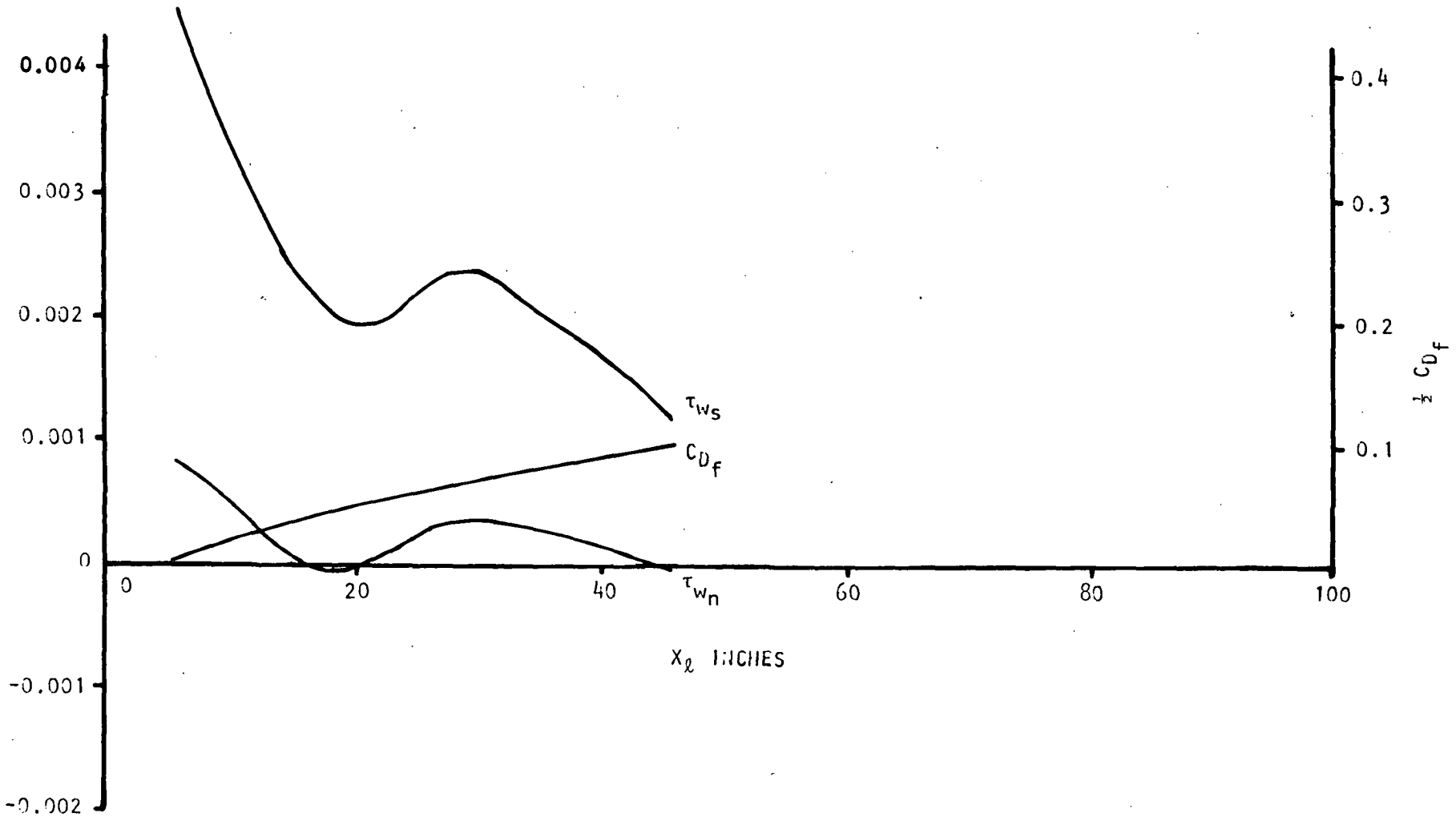

FIGURE 9 (Cont'd): 0.933 SEMISPAN

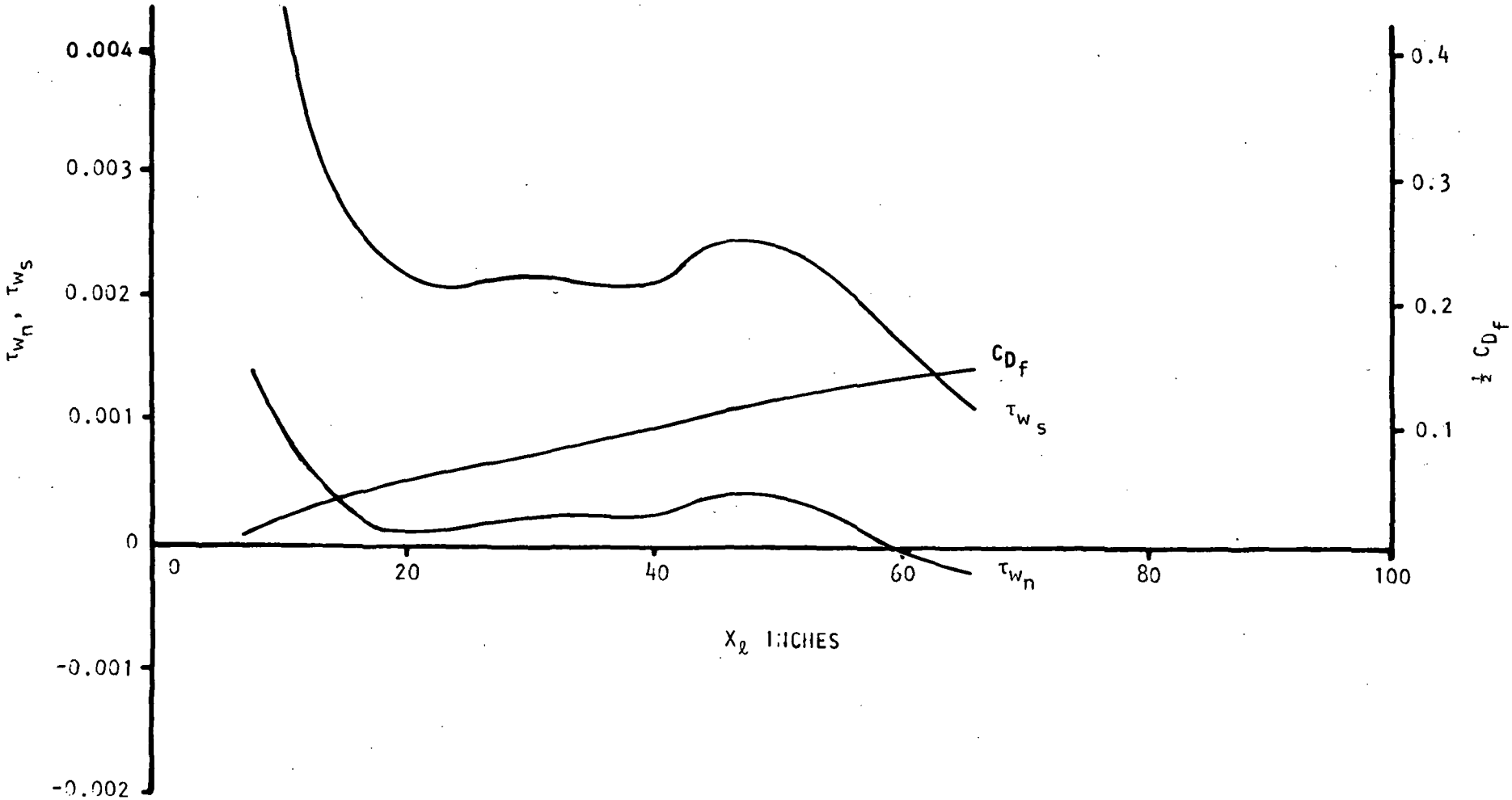

FIGURE 9 (Cont'd): 0.653 SEMISPAN

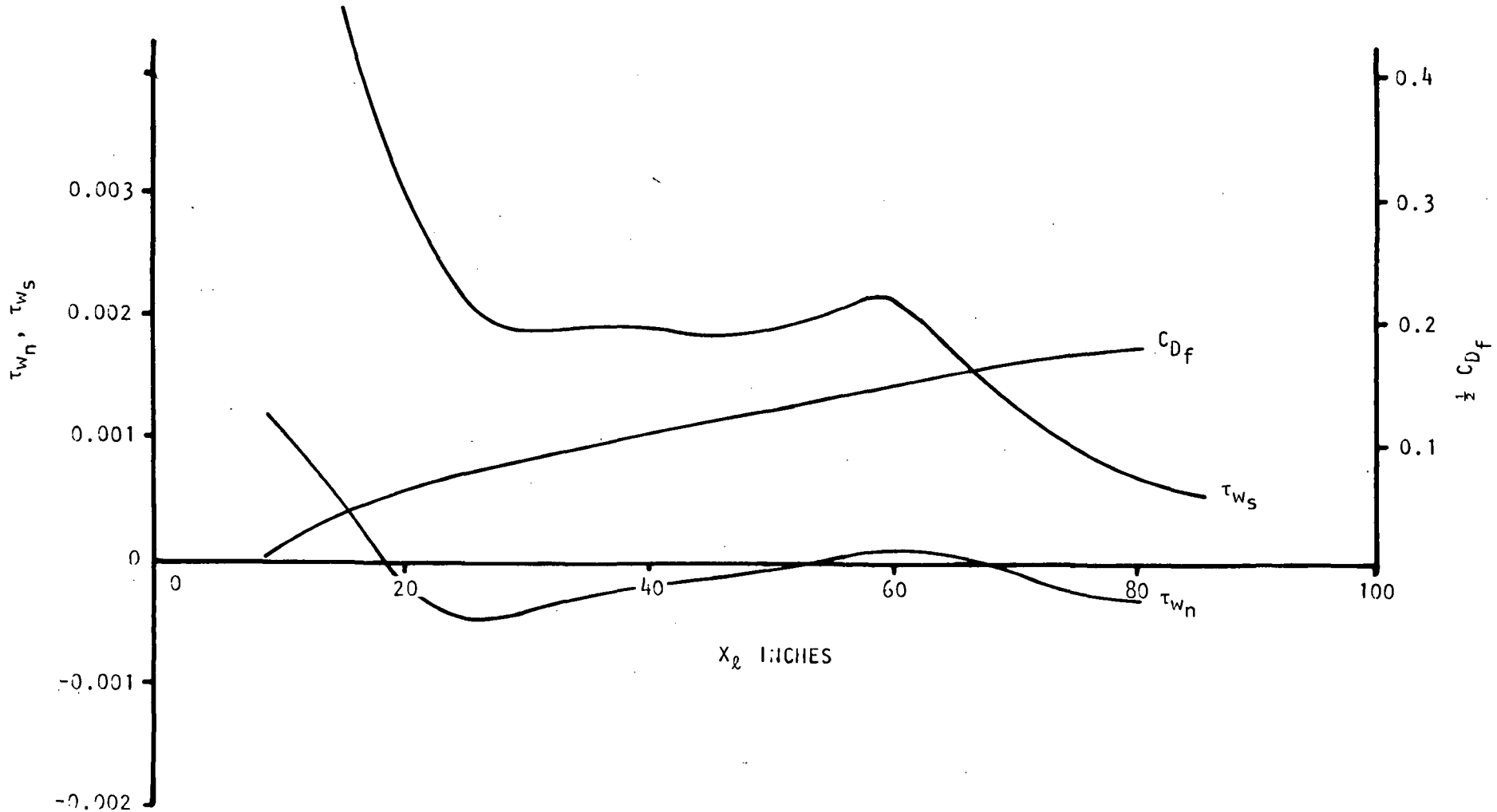

FIGURE 9 (Cont'd): 0.458 SEMISPAN

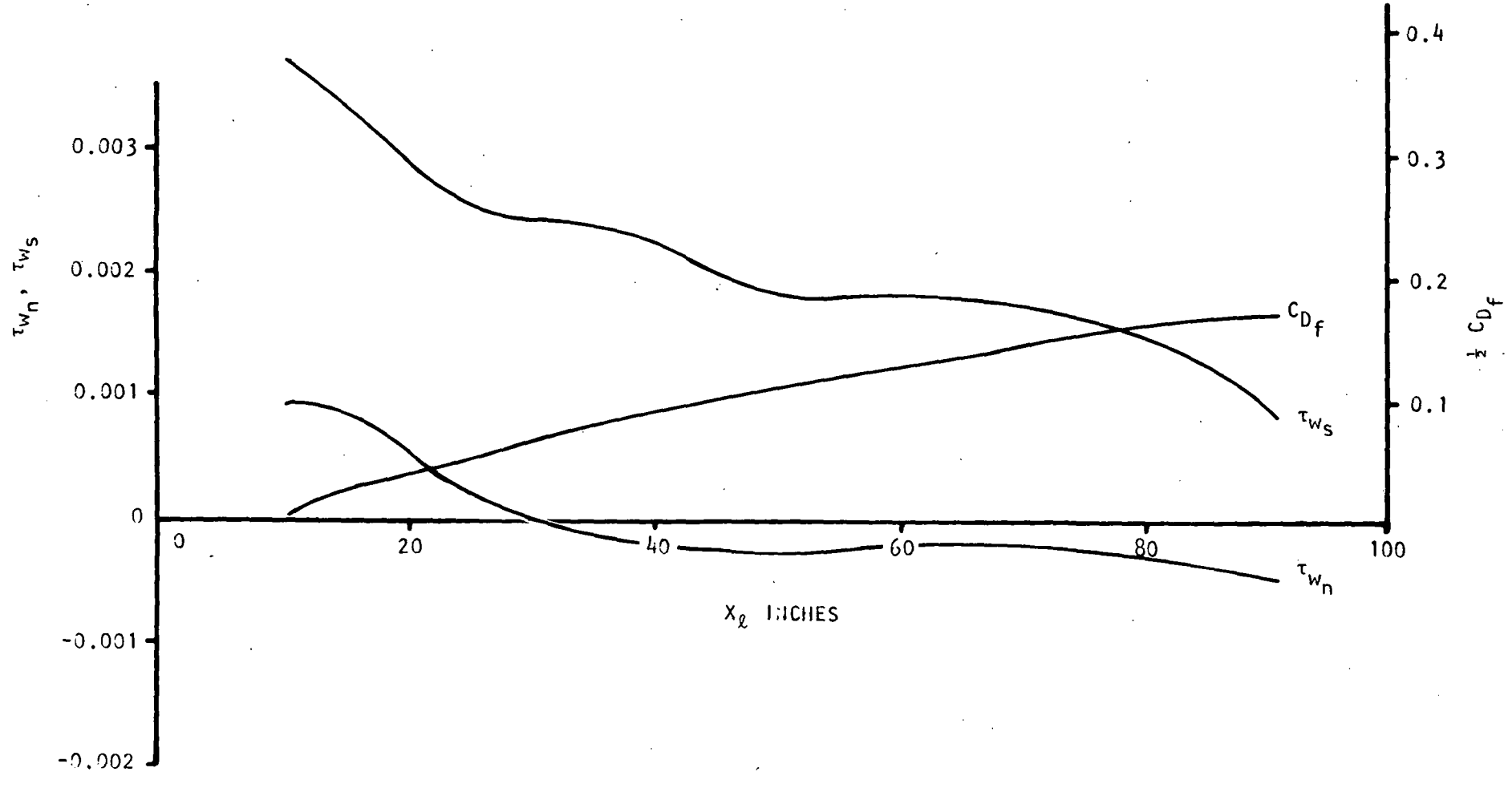

FIGURE 9 (Cont'd): 0.307 SEMISPAN

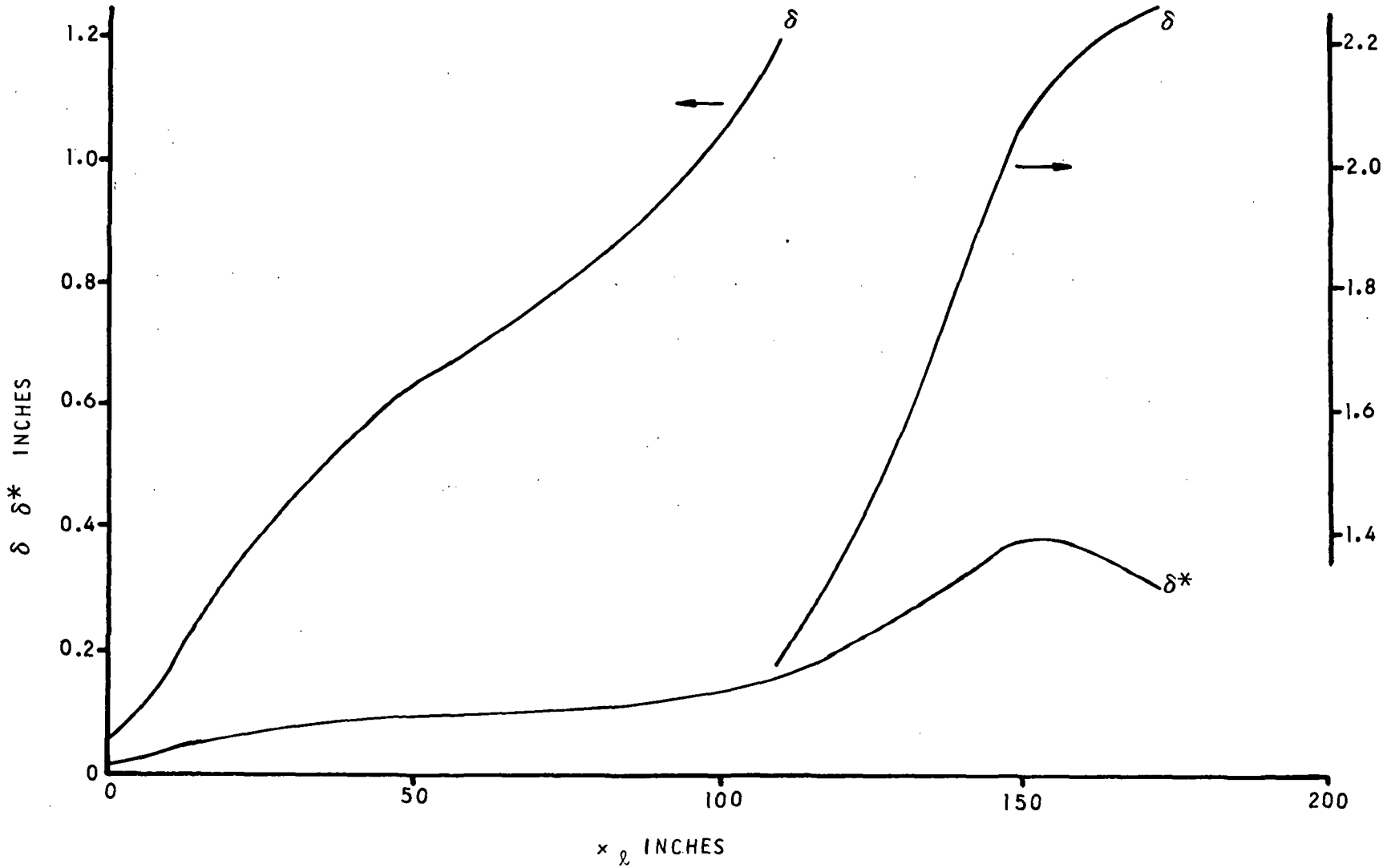

FIGURE 10 BOUNDARY-LAYER THICKNESS AND DISPLACEMENT THICKNESS, LOWER SURFACE: 0.133 SEMISPAN

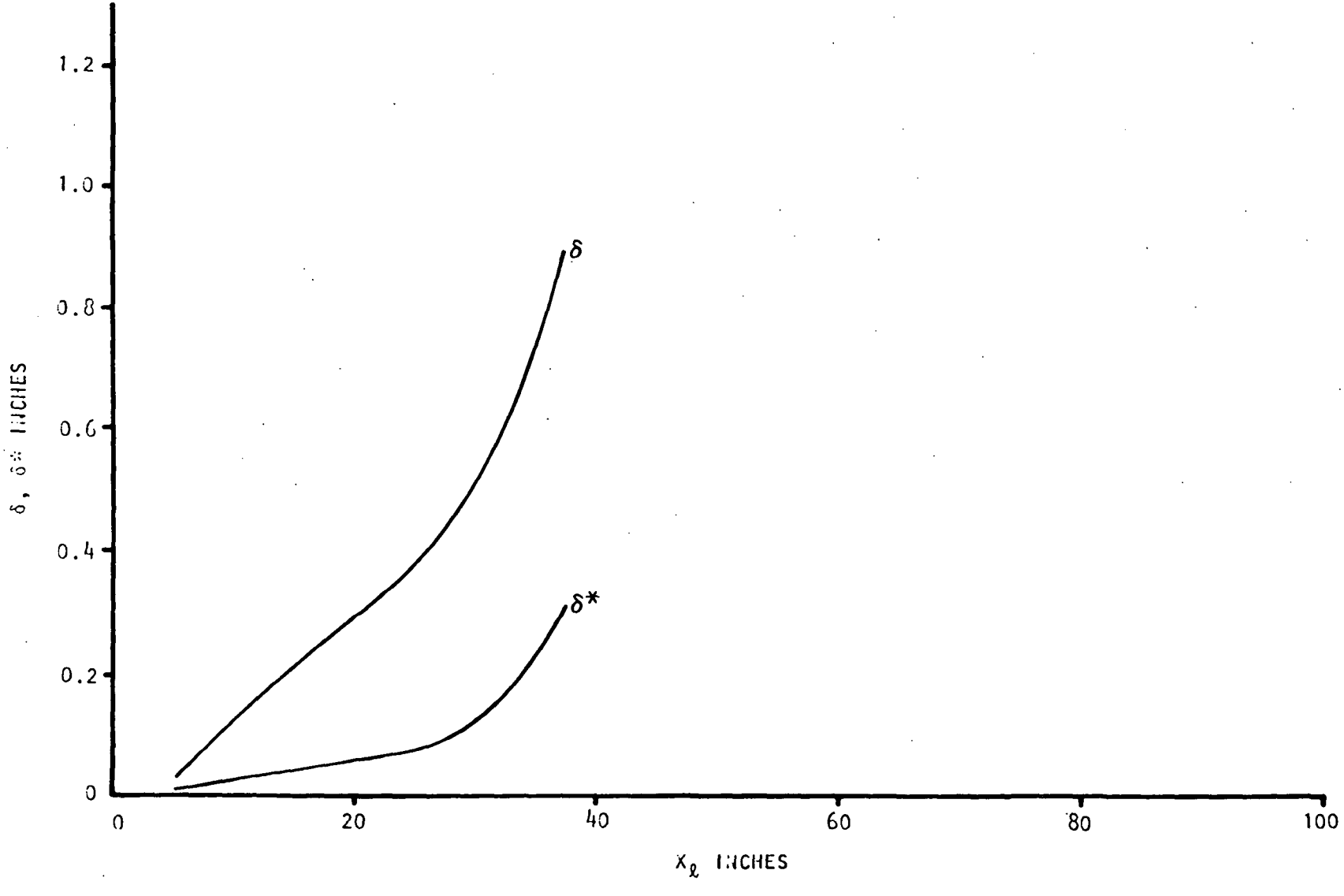

FIGURE 10 (Cont'd): 0.933 SEMISPAN

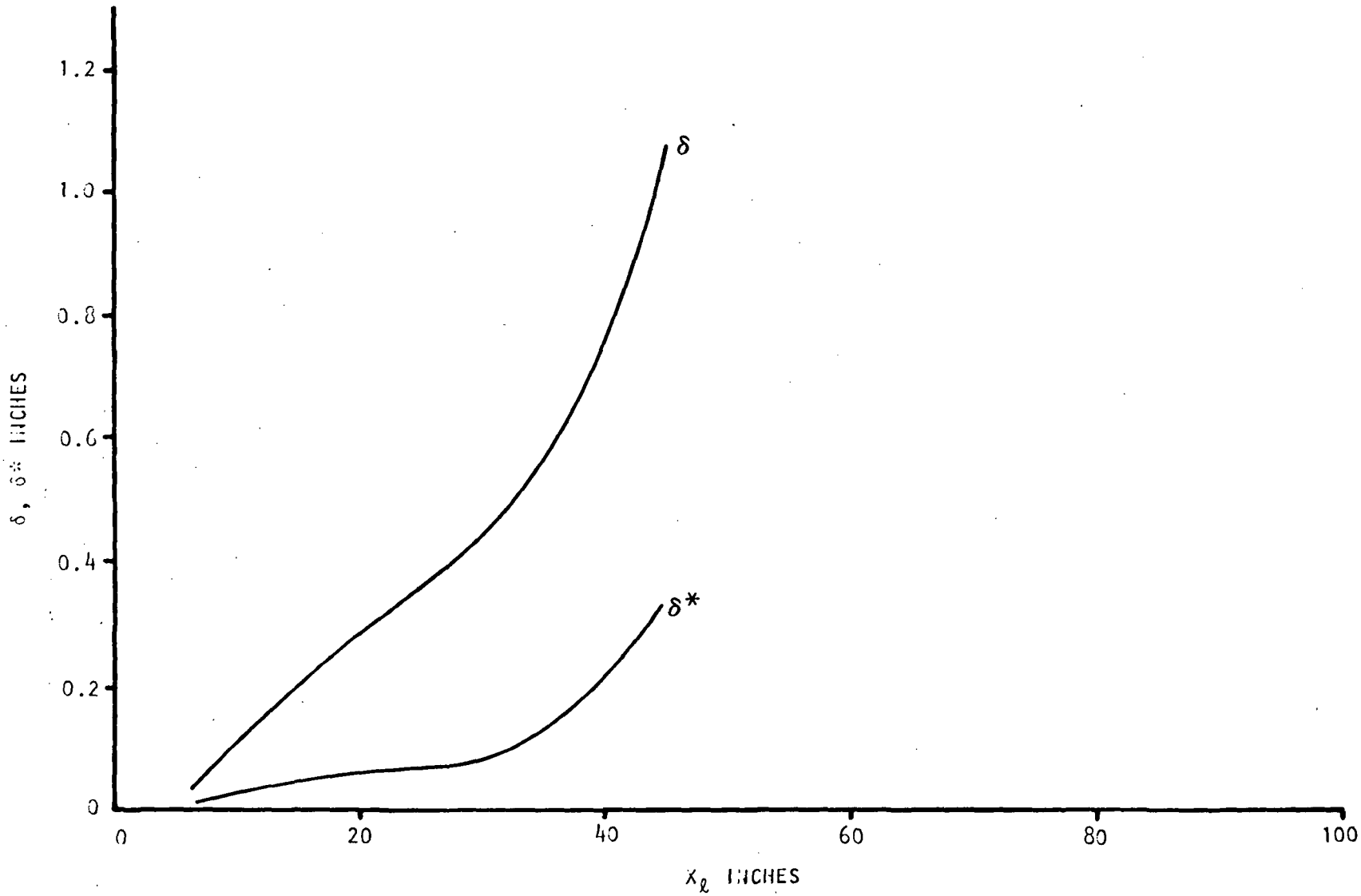

FIGURE 10 (Cont'd): 0.804 SEMISPAN

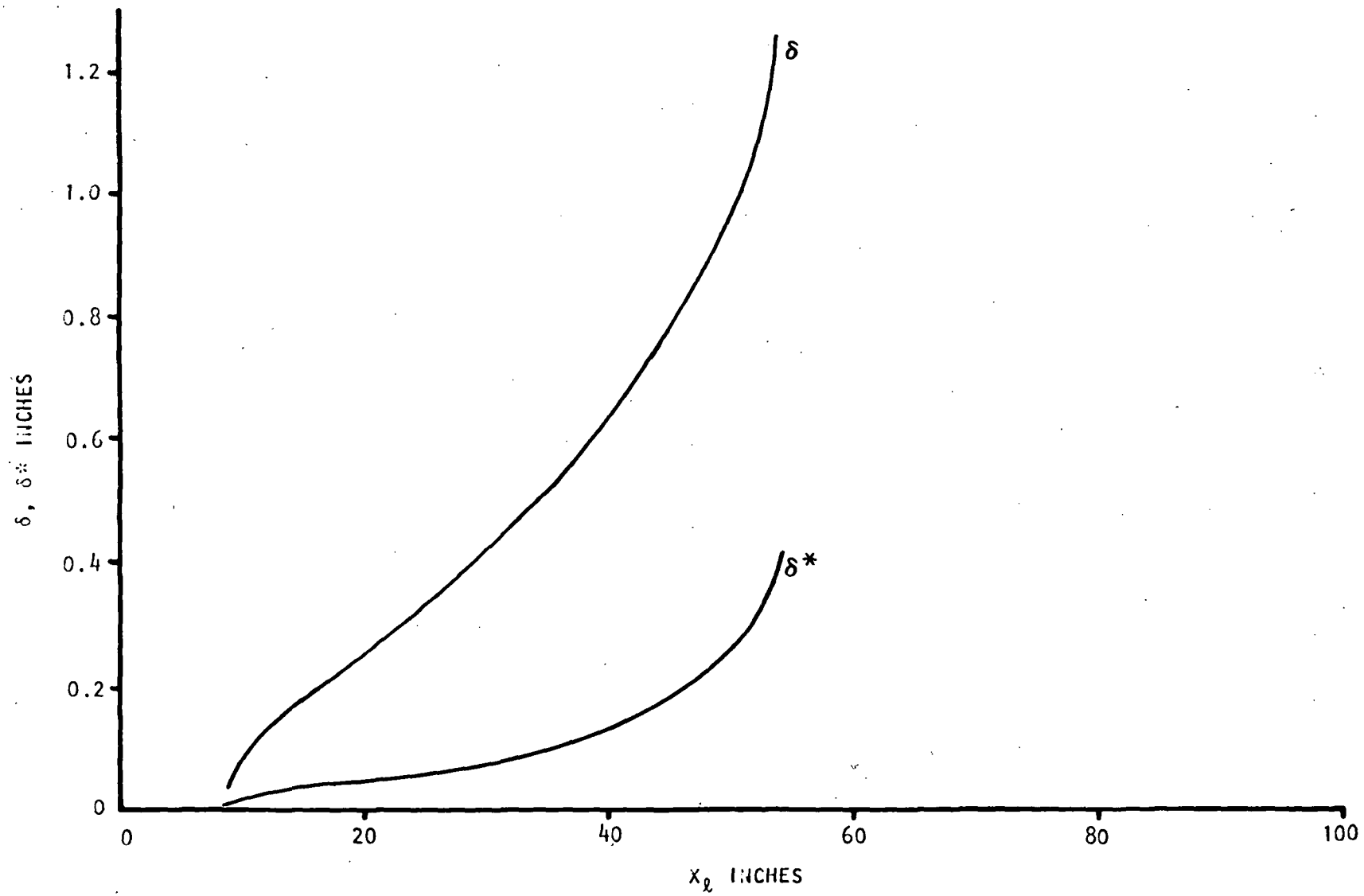

FIGURE 10 (Cont'd): 0.653 SEMISPAN

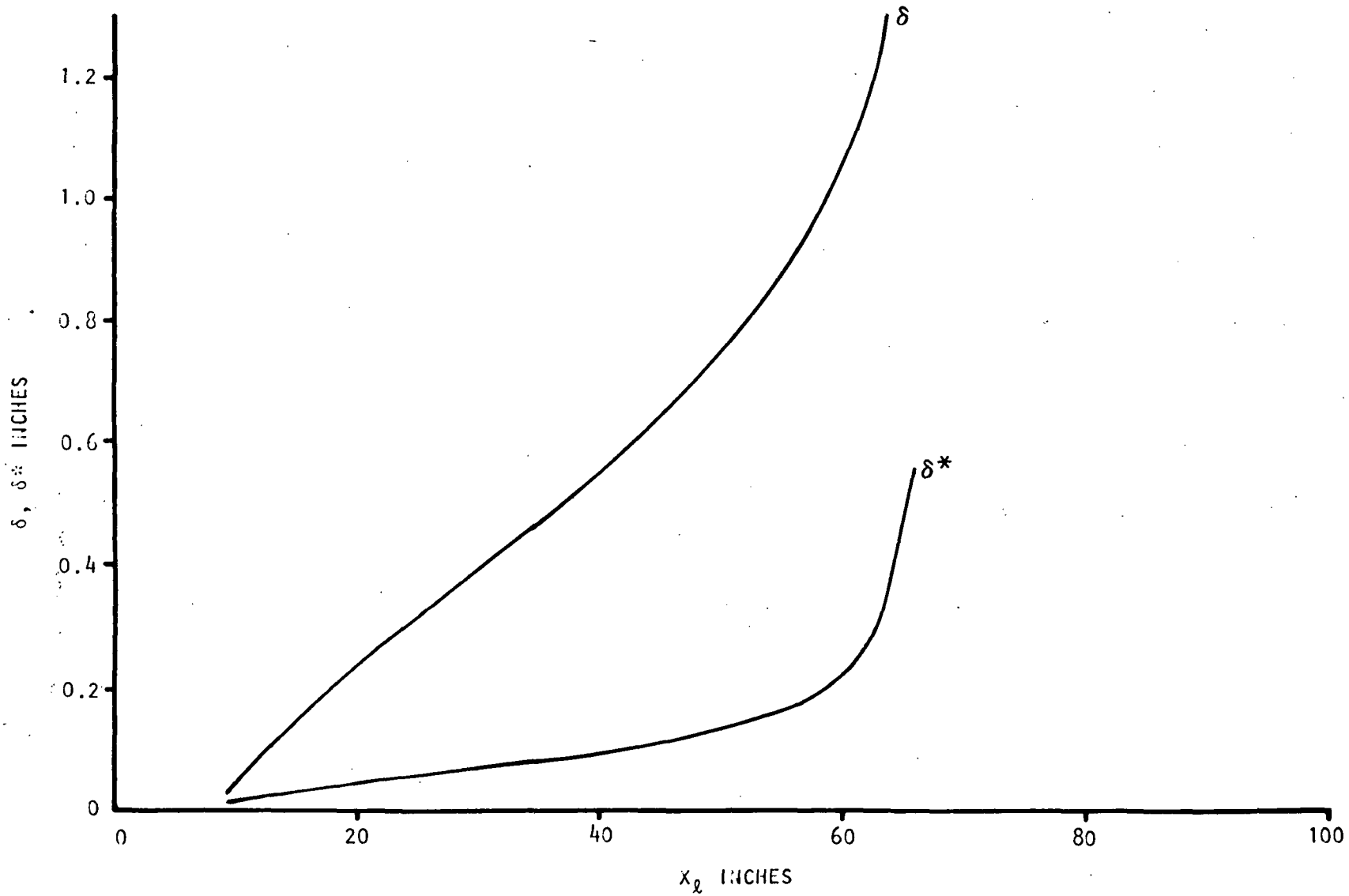

FIGURE 10 (Cont'd): 0.458 SEMISPAN

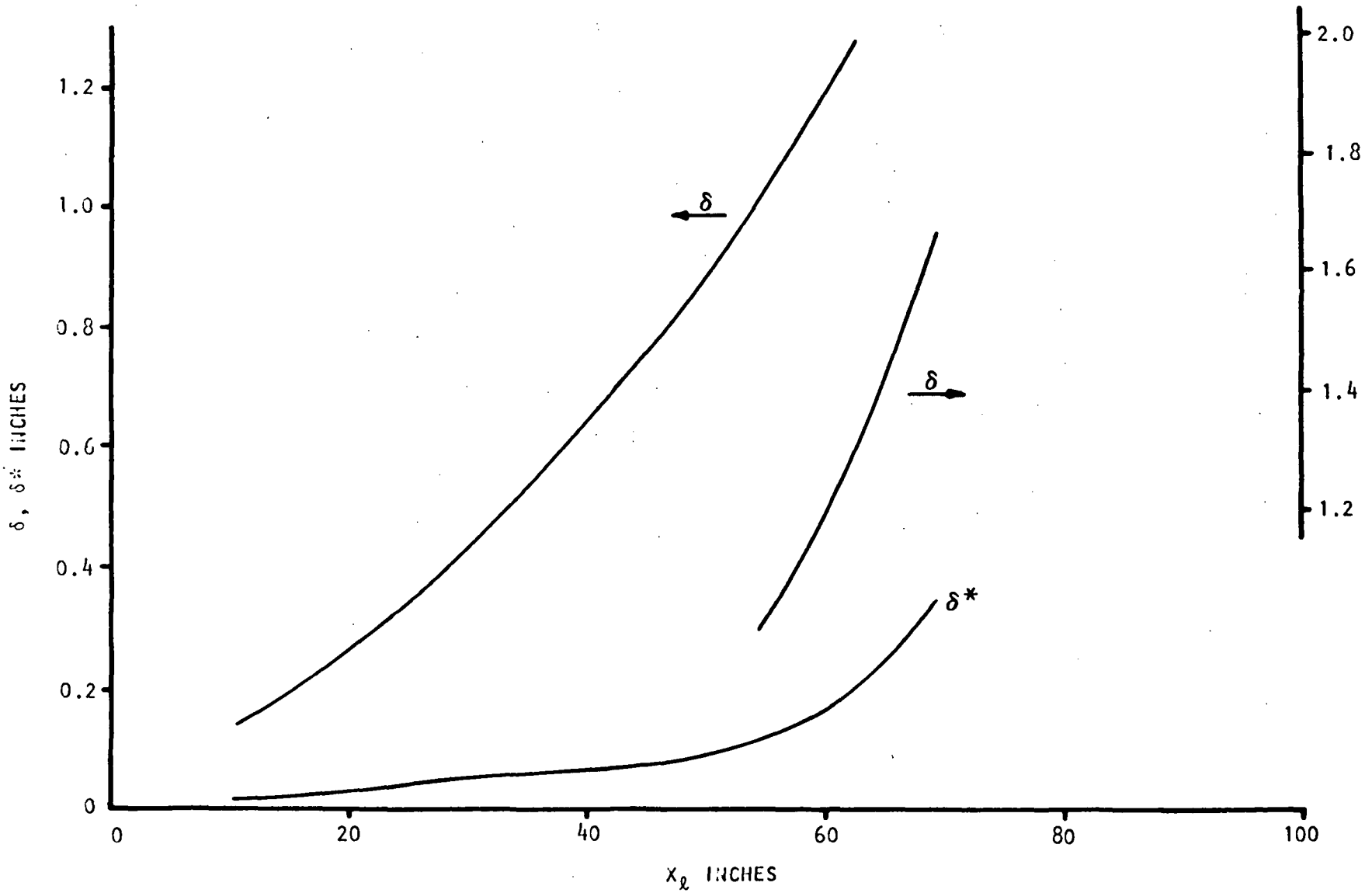

FIGURE 10 (Cont'd): 0.307 SEMISPAN

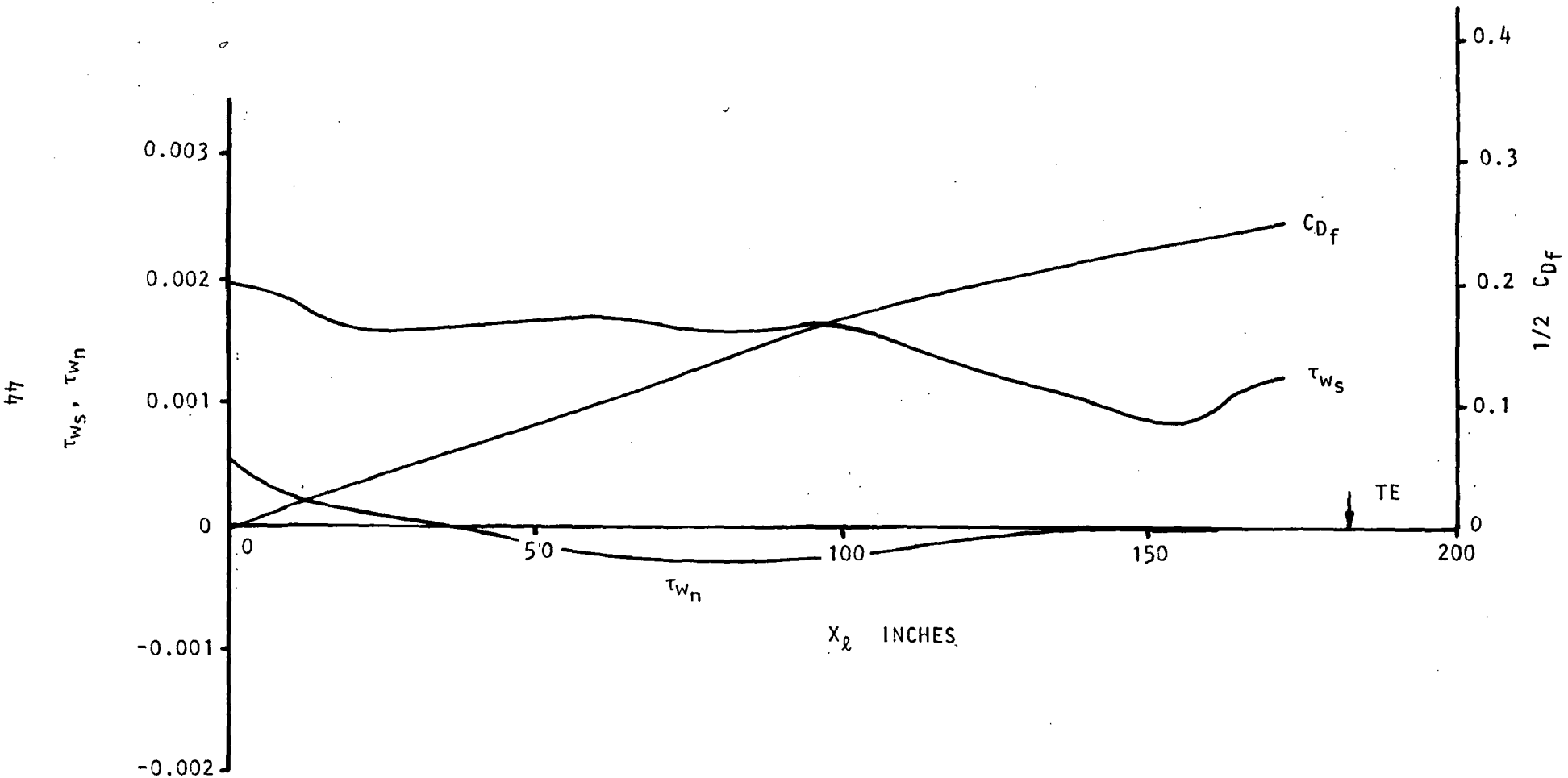

FIGURE 11 SKIN-FRICTION COMPONENTS AND INTEGRATED STREAMWISE SKIN FRICTION, LOWER SURFACE: 0.133 SEMISPAN

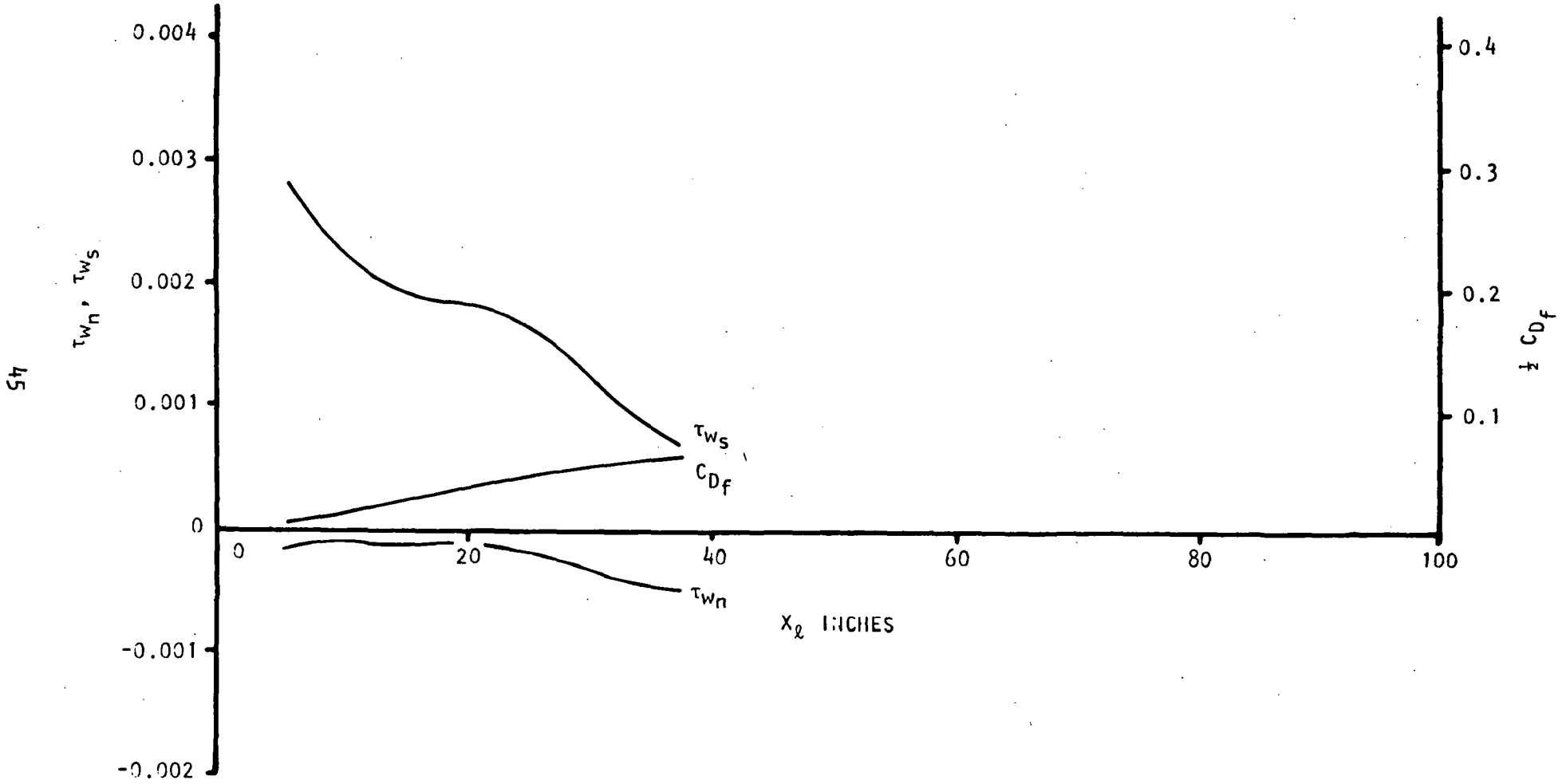

FIGURE 11 (Cont'd): 0.933 SEMISPAN

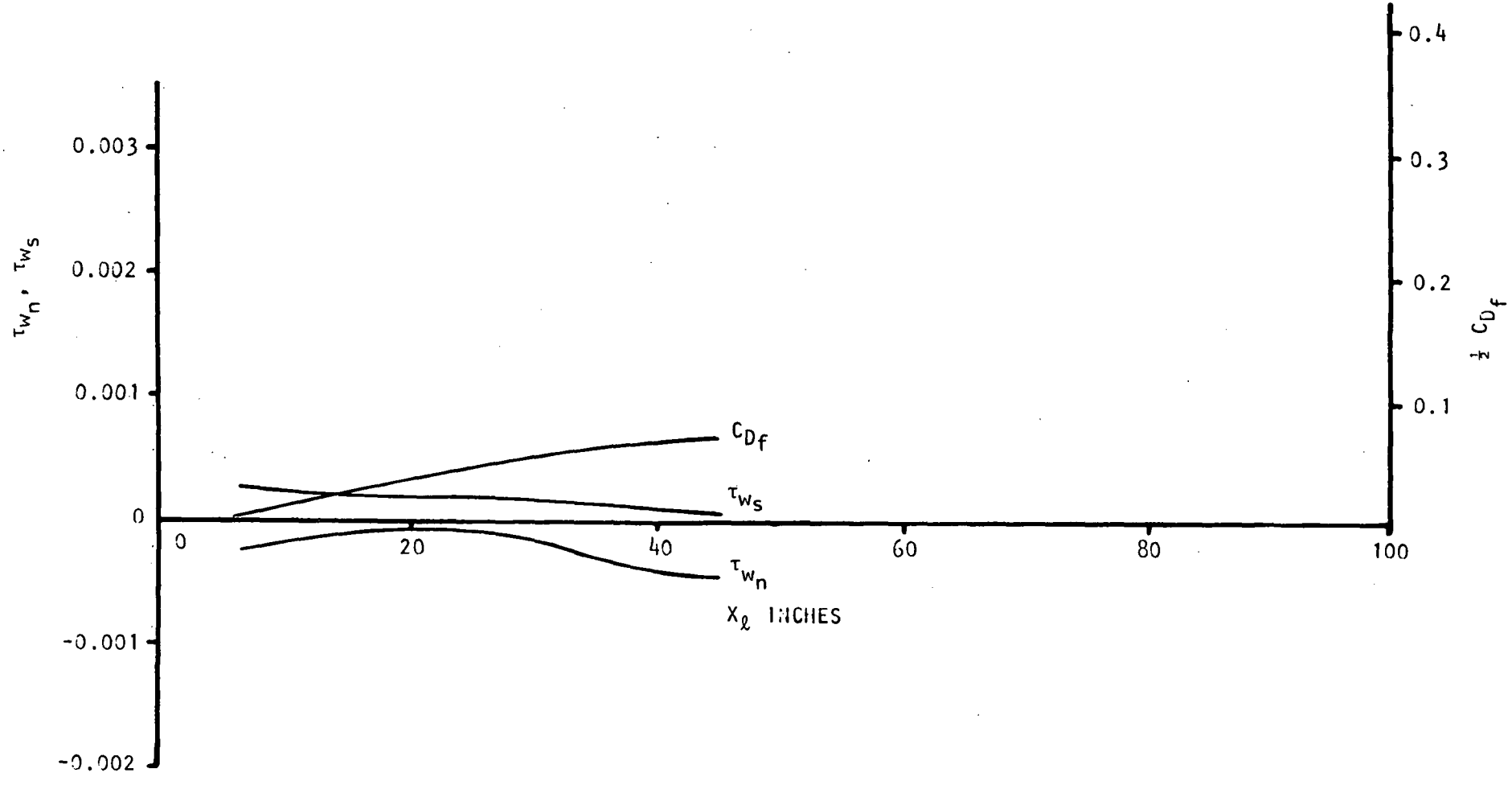

FIGURE 11 (Cont'd): 0.804 SEMISPAN

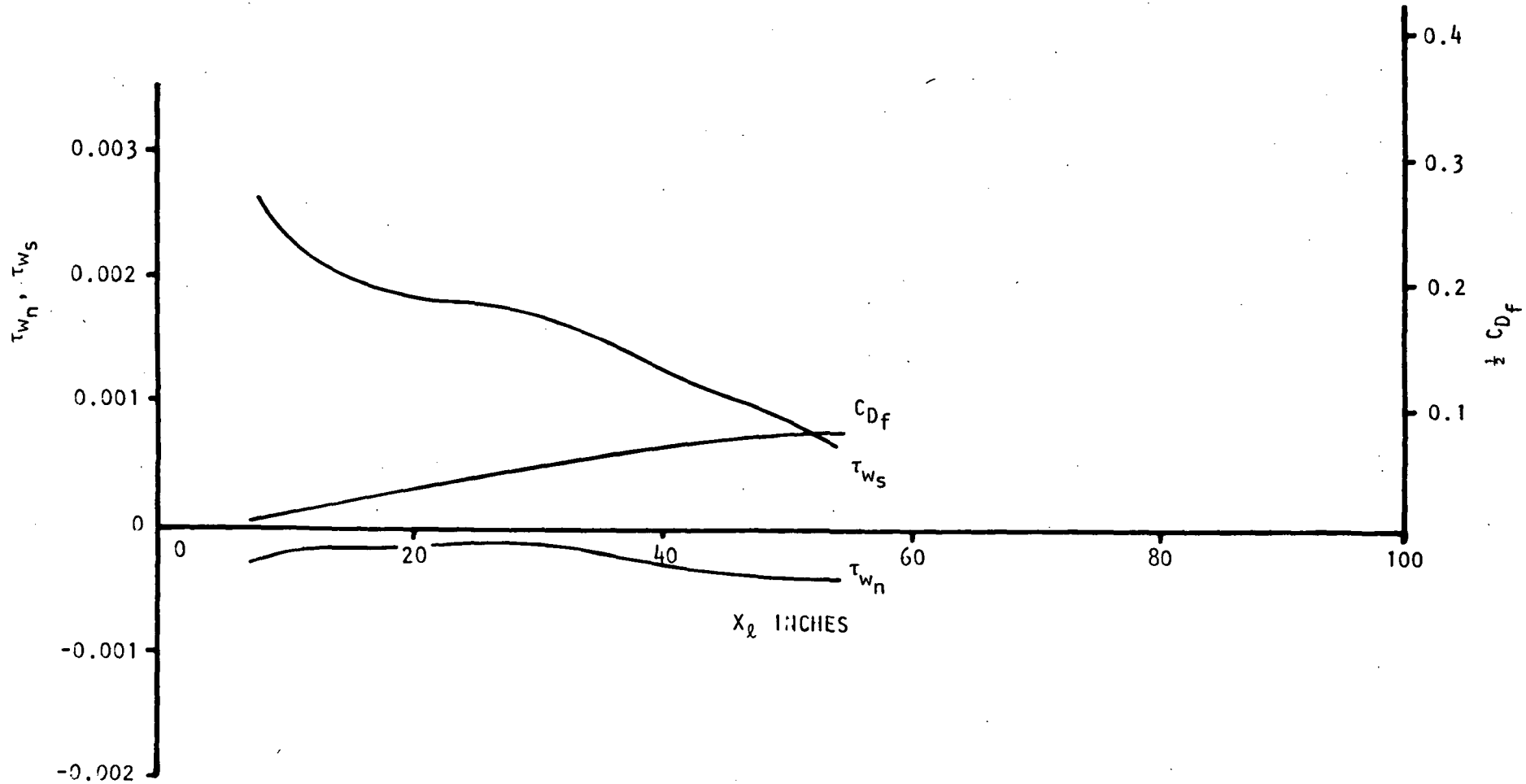

FIGURE 11 (Cont'd): 0.653 SEMISPAN

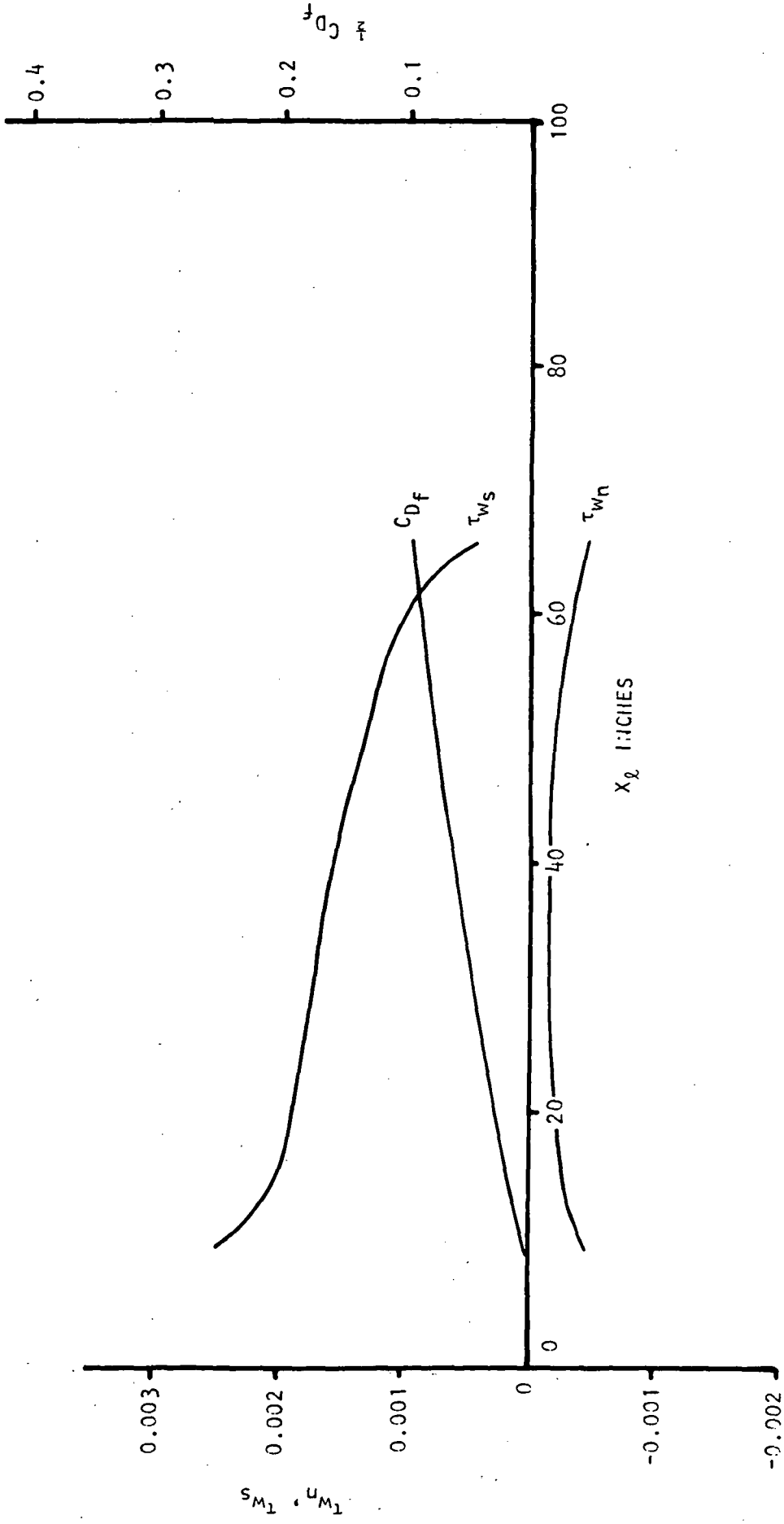

FIGURE 11 (Cont'd): 0.458 SEMISPAN

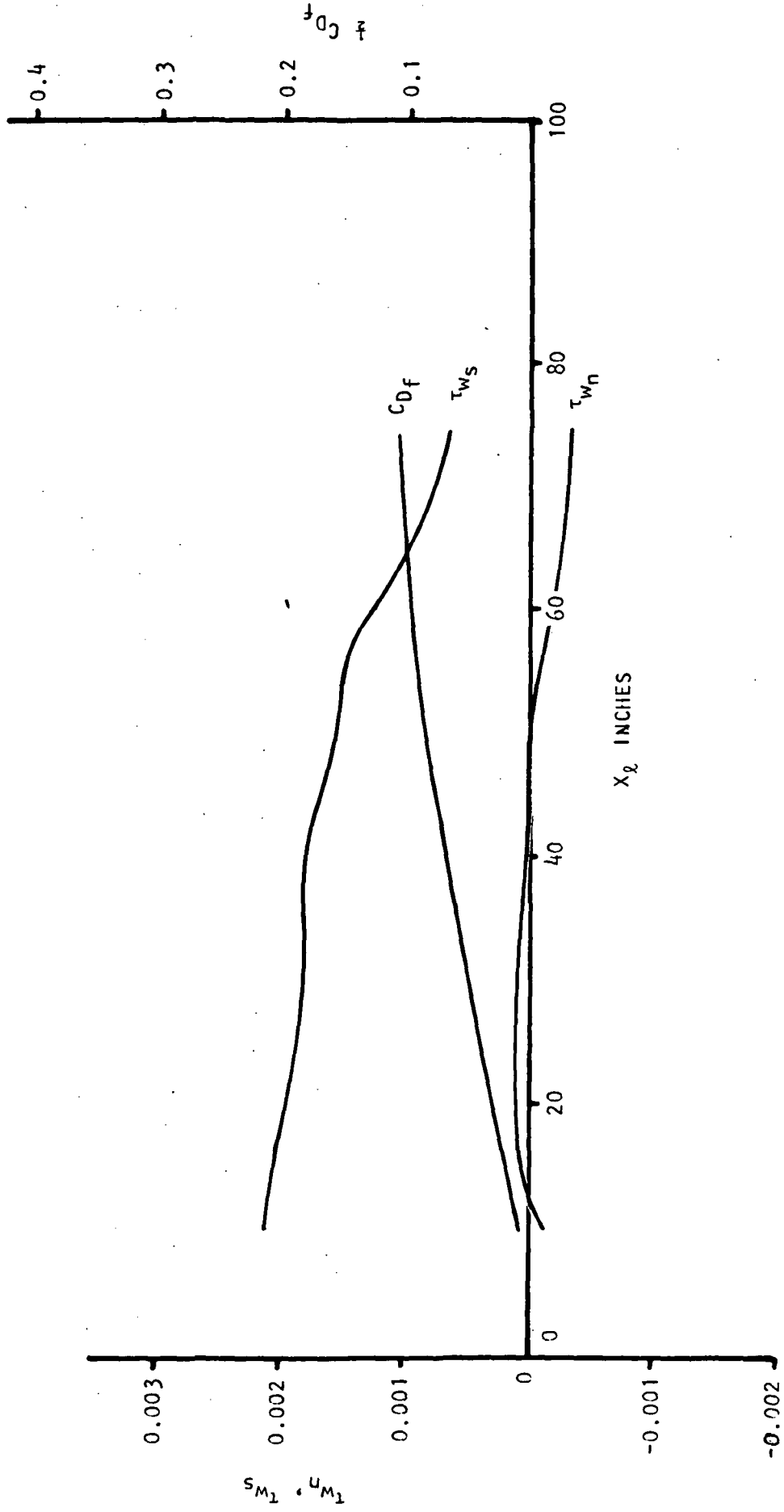

FIGURE 11 (Cont'd): 0.307 SEMISPAN

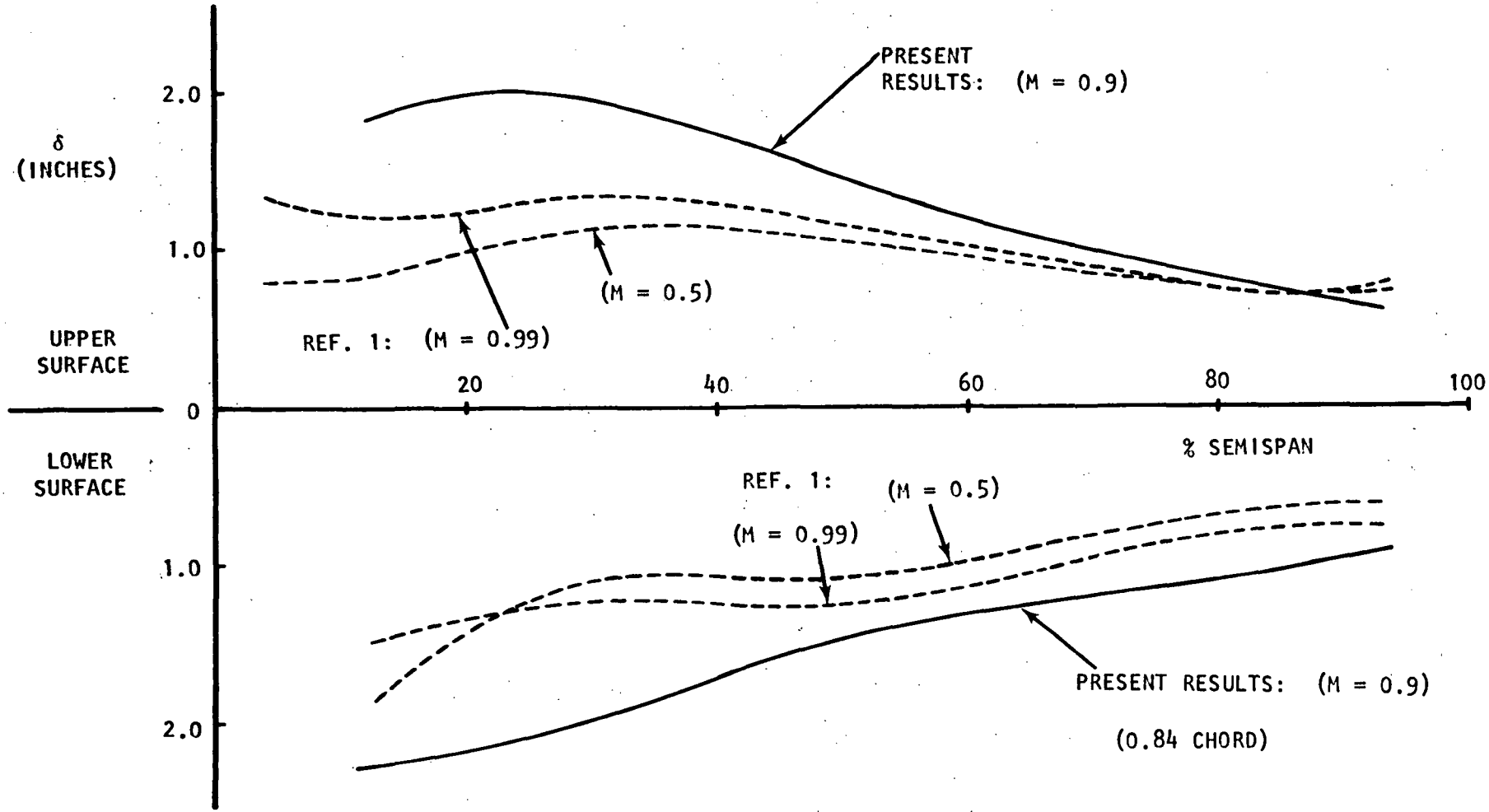

FIG. 12 BOUNDARY-LAYER THICKNESS AT THE TRAILING EDGE VERSUS SPANWISE POSITION

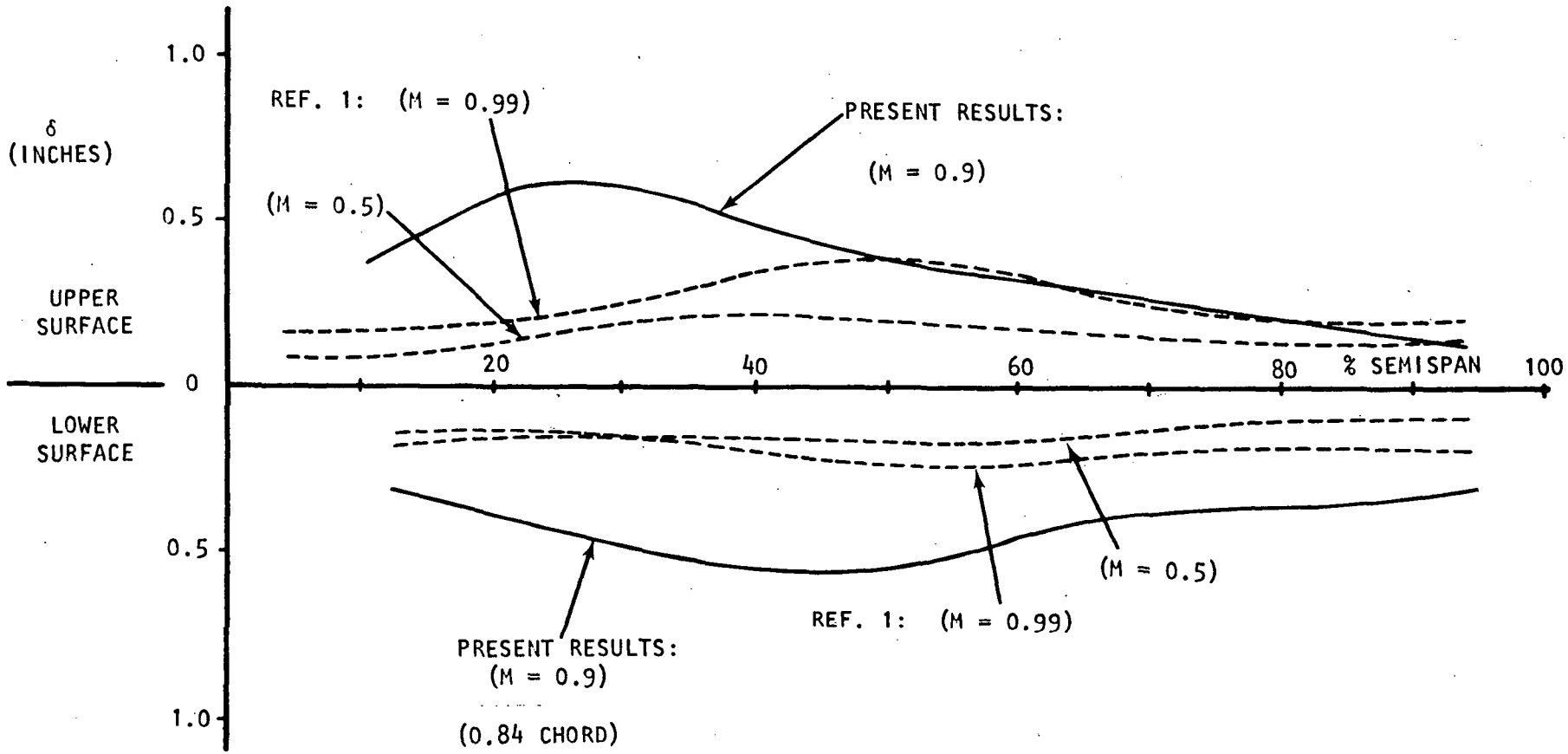

FIG. 13 DISPLACEMENT THICKNESS AT THE TRAILING EDGE VERSUS SPANWISE POSITION

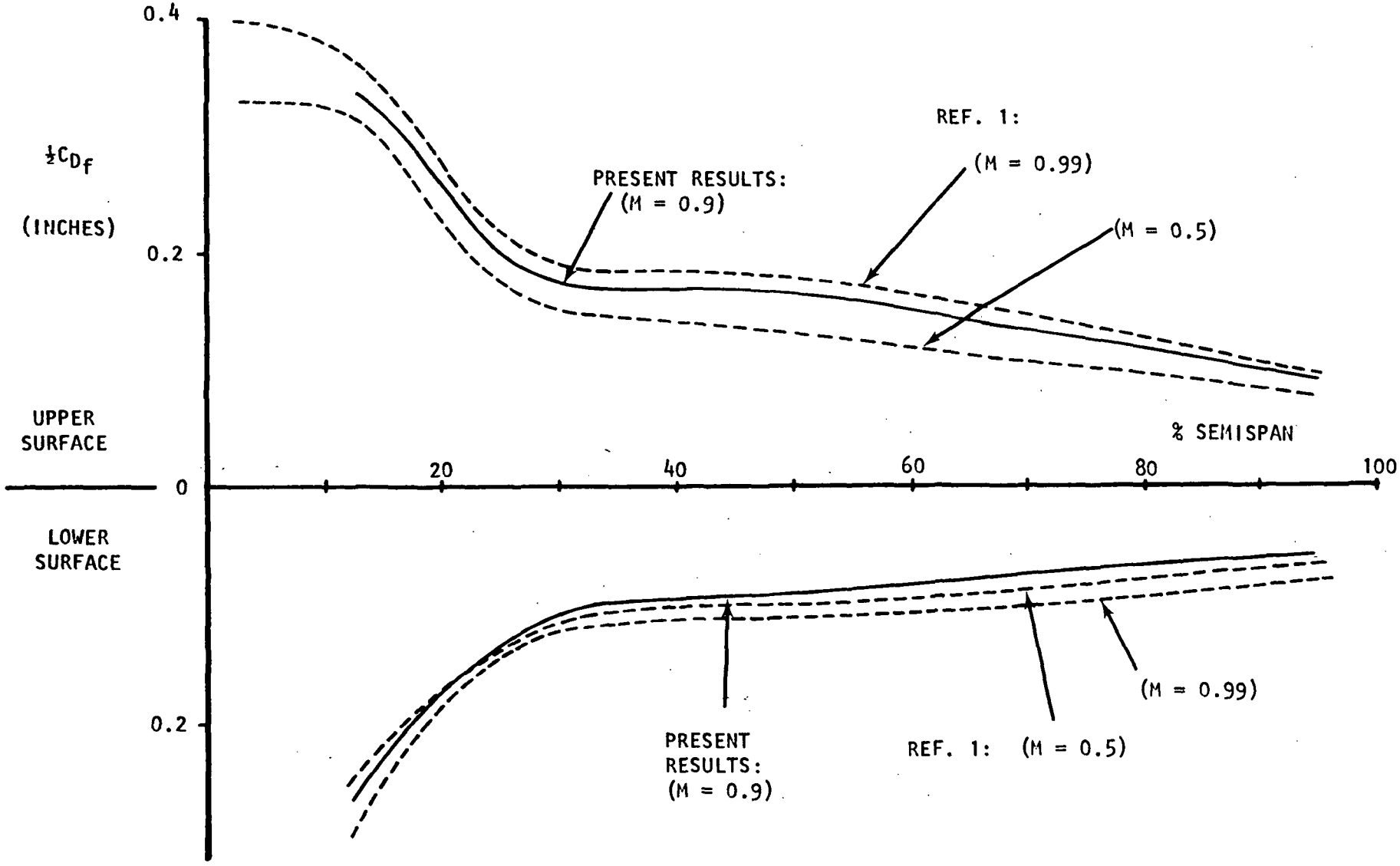

FIG. 14 INTEGRATED SKIN FRICTION AT THE TRAILING EDGE VERSUS SPANWISE POSITION

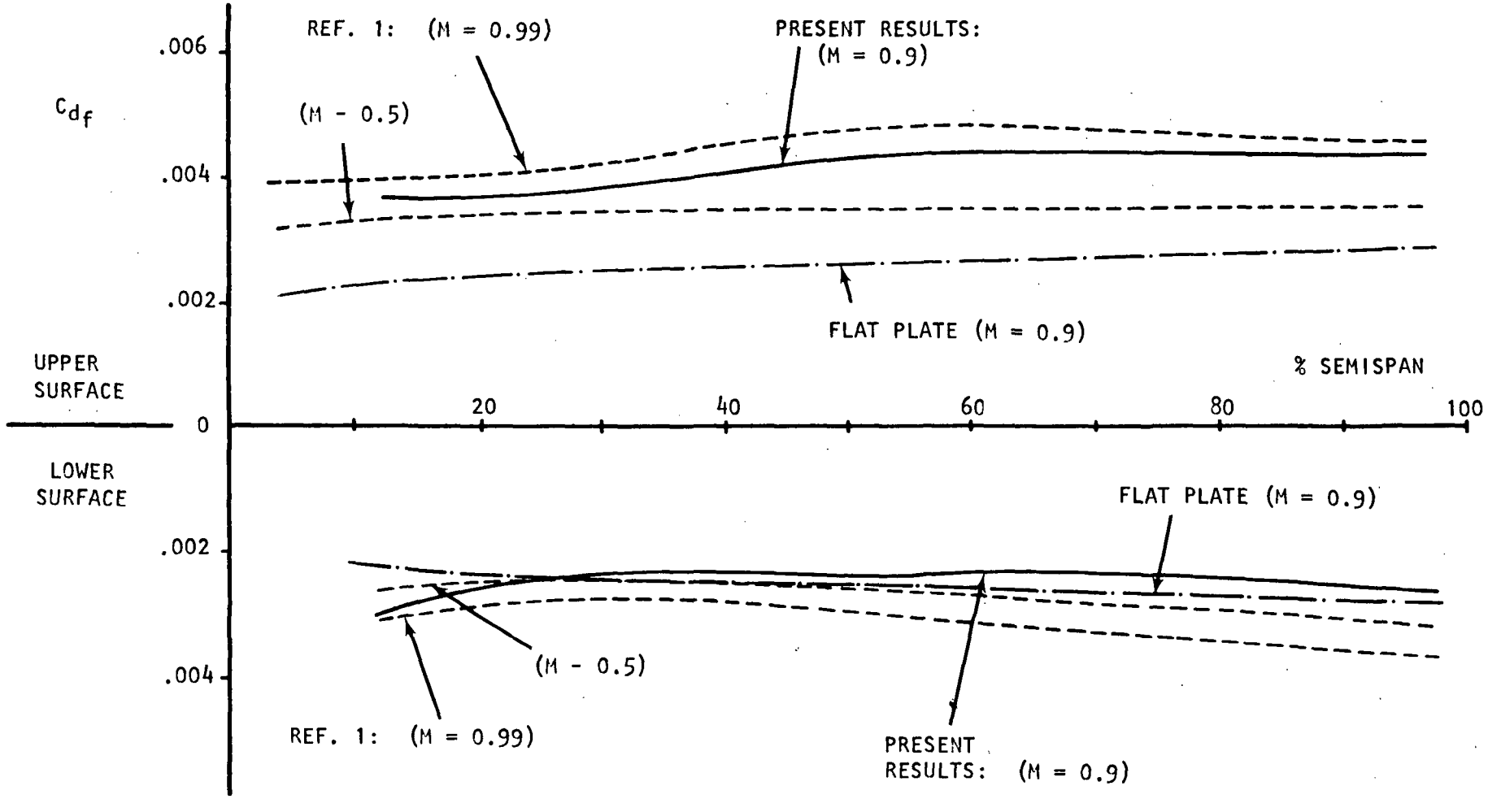

FIG. 15 SECTIONAL SKIN-FRICTION DRAG COEFFICIENT VERSUS SPANWISE POSITION

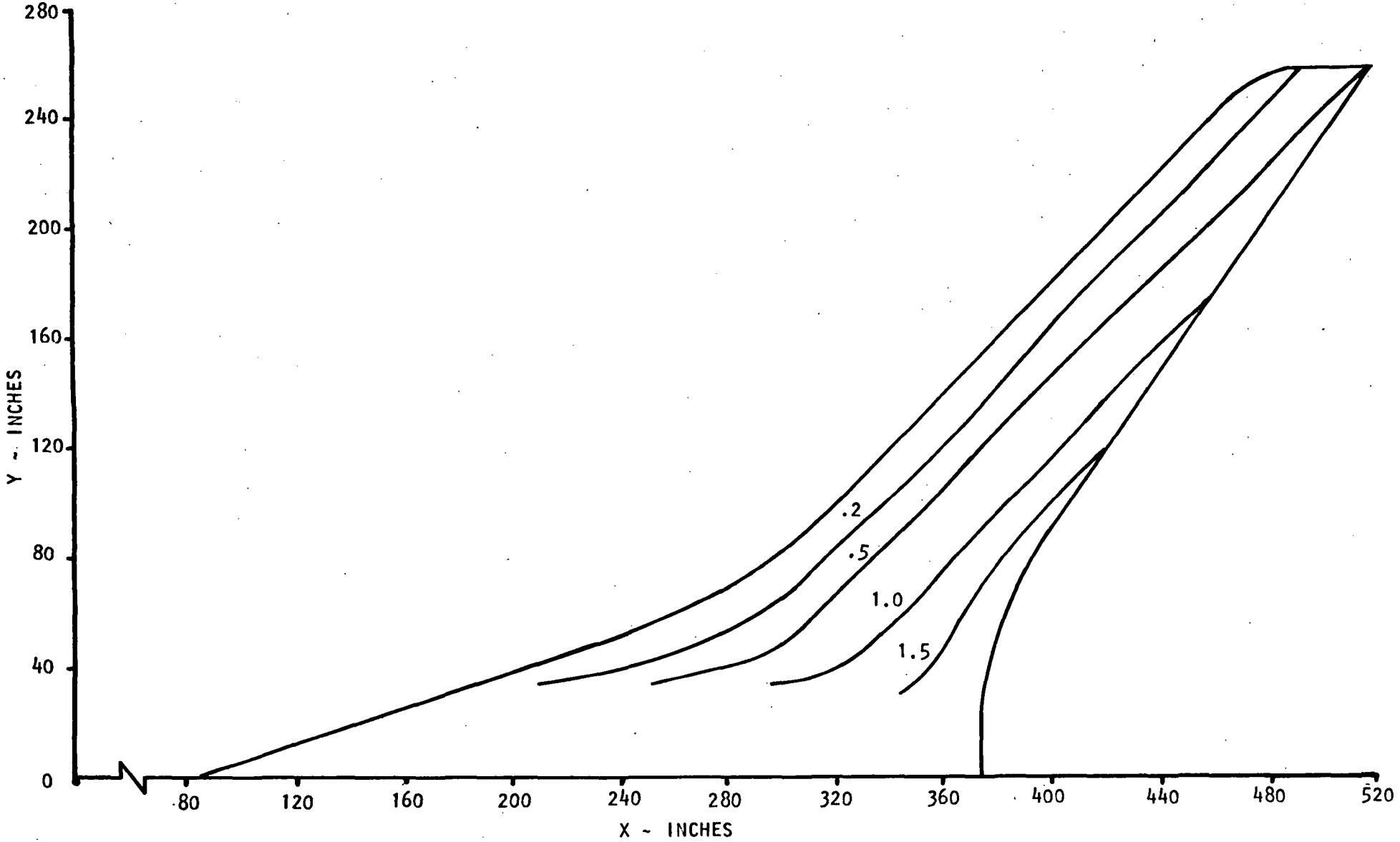

FIGURE 16 BOUNDARY LAYER THICKNESS CONTOURS, UPPER SURFACE

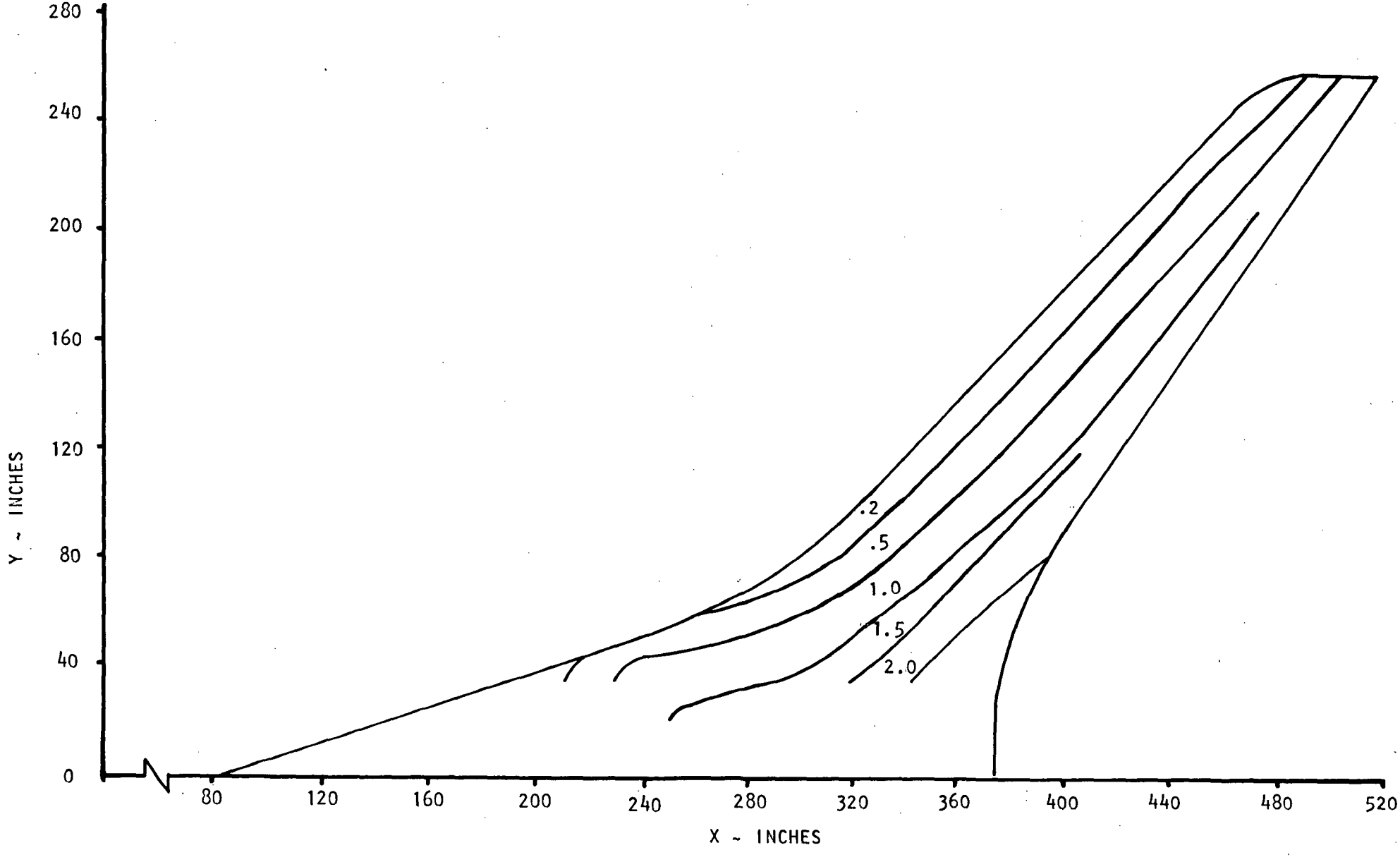

FIGURE 16 (Cont'd). LOWER SURFACE

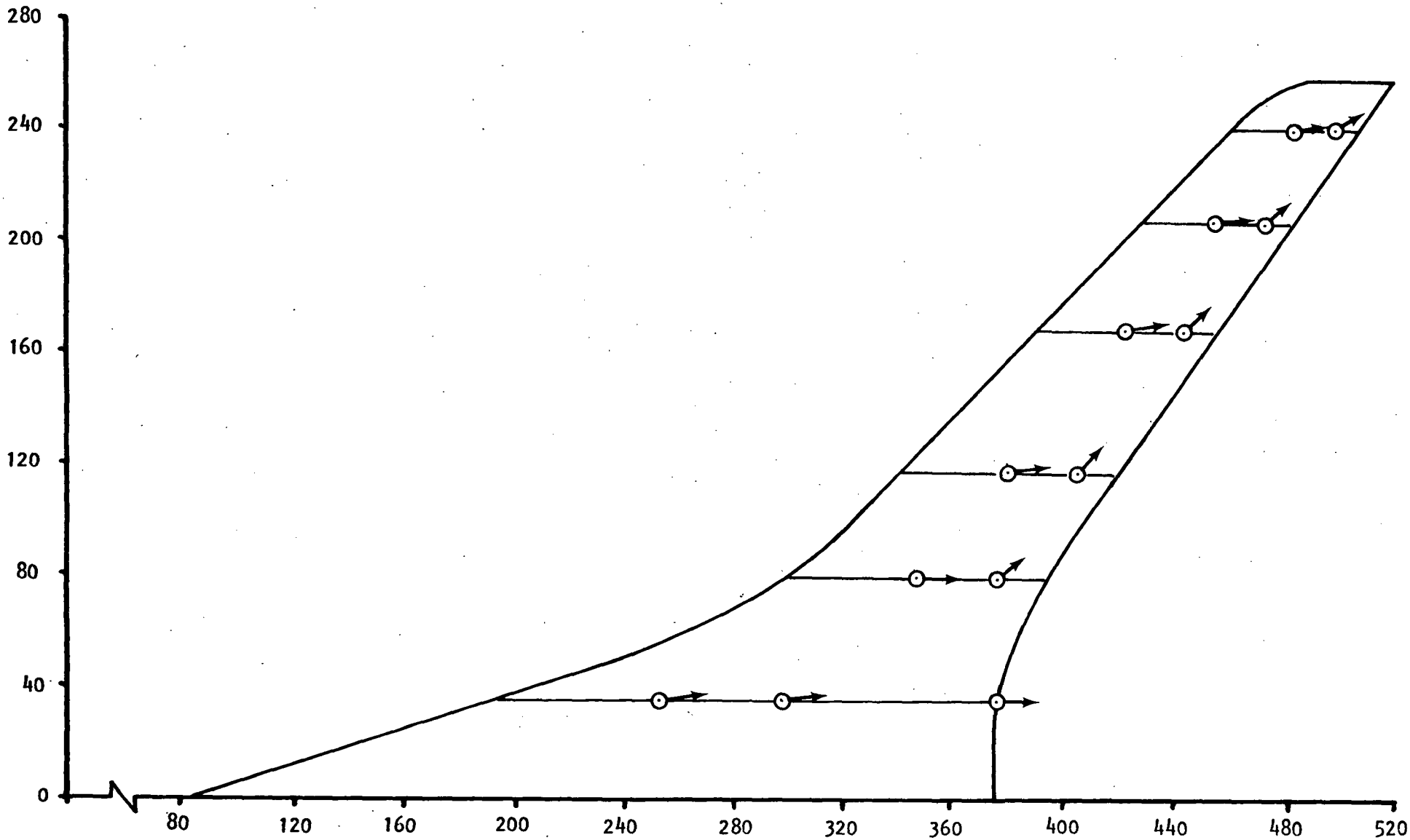

FIGURE 17 (Cont'd). LOWER SURFACE

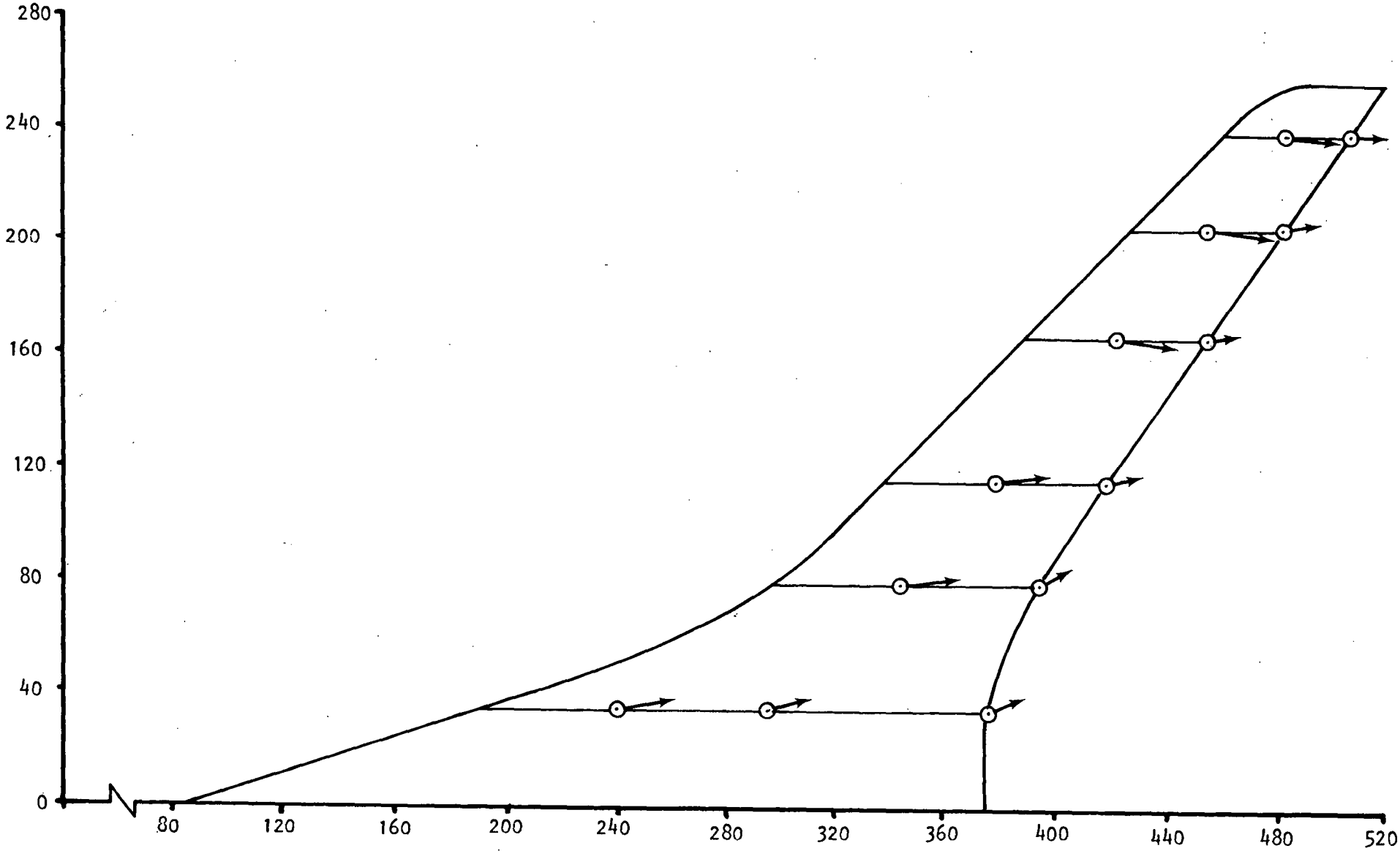

FIGURE 17. SURFACE STRESS VECTORS, UPPER SURFACE